Lectures presented at the 5th Nuclear Physics Summer School, Rudziska, Poland, Aug. 20-Sept. 2, 1972

LBL-1251

CORIOLIS EFFECTS IN NUCLEI

F. S. Stephens

September 1972

AEC Contract No. W-7405-eng-48

LBL-1251

DISCLAIMER

CORIOLIS EFFECTS IN NUCLEI*

F. S. Stephens

1. Introduction

Coriolis effects are not very common in our normal experience. Perhaps the most familiar object where these effects are large is the gyroscope or the "top", as the childhood-toy version is usually called. The sidewise precession of a leaning top under the influence of the downward pull of gravity is indeed a striking behavior, and one whose mystery testifies to our unfamiliarity with Coriolis effects. A less common example, but one much more analogous to the nuclear effects I want to discuss, is a ship's gyrocompass. In this case the tendency of a spinning gyroscope (whose axis is kept in the plane of the earth's surface) to align its axis with that of the rotating earth, is used as a navigational aid. A particle in an orbit of a rotating nucleus has a similar tendency, as we shall see. In the case of rotational nuclei, Coriolis effects are much more apparent than in our everyday experience, and it is the purpose of these lectures to examine what we know about such effects.

It is easy to estimate the maximum Coriolis energy of a particular particle in a rotating nucleus. For a particle orbit having angular momentum, j, in a nucleus with spin, I, and moment of inertia, $\mathcal{J}$, this energy is given by:

$$E_{Cor}(max) \approx 2 \frac{\hbar^2}{2\mathcal{J}} I\, j \quad . \tag{1}$$

In rare-earth nuclei there exist orbitals with j as large as 13/2, and $\hbar^2/2\mathcal{J}$ is around 0.01 MeV. Thus when I is only 7/2, the maximum Coriolis

* Work done under the auspices of the U.S. Atomic Energy Commission.

energy is almost 0.5 MeV, or quite comparable with the energy separations between particle states in such a nucleus. This indicates that for these favorable cases the Coriolis effects can be expected to affect the nuclear structure significantly even for such low spins. Equation (1) also shows clearly that these effects become larger with increasing spin and also with decreasing moment of inertia.

In the present lectures I want to review the Coriolis effects in nuclei, beginning with cases where they are relatively small; that is, good rotational nuclei (small $\hbar^2/2\mathcal{I}$), low-j orbitals, and relatively low spin values. An example of this type is the famous case of ^{183}W. Then I want to proceed to some intermediate cases where j is large, I is moderately large, but $\hbar^2/2\mathcal{I}$ remains small (rotational nuclei). These cases are ^{235}U and the odd-A Er nuclei. With these as background I will then describe two situations that we have proposed might correspond to cases where the Coriolis effects have changed the nuclear structure in a major way. The first of these is the case where j is large, I is moderately large, and $\hbar^2/2\mathcal{I}$ becomes large; that is, in the more "vibrational" nuclei. I will consider mainly the odd-A La, Au, and Tl nuclei in this category. The other situation is that of very large I ($\sim$20) in rotational nuclei, where these effects can be shown to provide one possible explanation for the peculiar behavior recently observed in even-even nuclei. Throughout these discussions I will try to emphasize the physical effects occurring rather than the mathematical detail, although some of the latter will be essential.

It is important to keep in mind that in all these cases we are treating just <u>one</u> physical system, a particle coupled to a core that is deformed and can rotate. In the first cases I will discuss, the deformation of the core is large

and the particle is strongly coupled to it so that as the core rotates the particle follows. The Coriolis effects are then a small perturbation on the rotational spectra. In the last cases, the coupling to the deformed shape is weak and/or the rotational frequencies are large, so that the particle cannot follow the core rotation, resulting in Coriolis effects that completely obscure the simple rotational bands. It is certainly true that at some point, as the coupling decreases (β gets smaller), this rotational model will cease to apply to nuclei, but in order to find that point we must first understand just what the model implies clear down to the limit of zero coupling. Furthermore, there is some intriguing experimental evidence that suggests the model applies rather well at surprisingly weak couplings for at least some special states.

2. Coriolis Effects as Perturbations in Rotational Spectra

2.1. ^{183}W

A. Bohr[1]) discussed Coriolis effects in his original paper on nuclear rotation in 1952, but it was some four years later before A. K. Kerman[2]) applied these ideas to a specific case, namely ^{183}W. I want to begin with this case, both because of its historical interest, and because it illustrates the effects in a simple case where only two bands are involved. The basic equations necessary to understand nuclear Coriolis effects are very simple, provided the deformed core is assumed to be axially symmetric and furthermore that $K = \Omega$ for all the low-lying states. The Hamiltonian of the system can be written:

$$H = H_p + \sum_i \frac{\hbar^2}{2\mathcal{J}_i} R_i^2 = H_p + \frac{\hbar^2}{2\mathcal{J}} \vec{R}^2 = H_p + \frac{\hbar^2}{2\mathcal{J}} (R_x^2 + R_y^2), \qquad (2)$$

where H_p is the Hamiltonian of the particle in the absence of rotation (a Nilsson[3]) Hamiltonian for example), $\mathcal{I}$ is the moment of inertia of the axially-symmetric core, and $\vec{R}$ is the rotational angular momentum of the core (rotation is not allowed around the symmetry axis). A coupling between the particle and the rotation comes about through the sharing of the total angular momentum between the particle and the core. This can be expressed by:

$$\vec{R} = \vec{I} - \vec{j} \quad . \tag{3}$$

One should clearly distinguish between the particle-rotation coupling which we are discussing, and the particle-core coupling, which is contained in H_p. (The major part of the particle-core coupling is spherically symmetric and of no interest here; however, if the core is deformed, then there is also a coupling to the deformation, which we discussed at the end of the previous section.) Putting eq. (3) into eq. (2), gives the usual expression for the rotational nucleus:

$$H = H_p + \frac{\hbar^2}{2\mathcal{I}}\left[I(I+1) - K^2\right] + H_c + \frac{\hbar^2}{2\mathcal{I}}\left[\langle \vec{j}^2 \rangle - \Omega^2\right] \quad , \tag{4}$$

where H_c is the Coriolis operator which is given by:

$$H_c = -2\,\frac{\hbar^2}{2\mathcal{I}}\left[\vec{I}\cdot\vec{j} - \Omega^2\right] = -\frac{\hbar^2}{2\mathcal{I}}\left[I_+ j_- + I_- j_+\right] \quad . \tag{5}$$

These are the general equations which we will use repeatedly later on, but for the present case of good rotational nuclei they can be further simplified. For such cases, Ω is a constant for a given band, as is $\langle \vec{j}^2 \rangle$. These may therefore be included in H_p, giving:

$$H = H_p' + \frac{\hbar^2}{2\mathcal{J}}\left[I(I+1)\right] + H_c \quad . \tag{6}$$

The matrix elements of H_c can be written:

$$\langle I,\Omega\pm1 \,|H_c|\, I,\Omega\rangle = -\frac{\hbar^2}{2\mathcal{J}}\sqrt{(I\mp K)\,(I\pm K+1)}\;\;\langle \Omega\pm1|j_\pm|\Omega\rangle \quad , \tag{7}$$

where the matrix element, $\langle\, \Omega\pm1|j_\pm|\Omega\,\rangle$, must, in general, be calculated from the detailed (e.g. Nilsson) wave functions. For the special case where j is a good quantum number, these can be written:

$$\langle j,\Omega\pm1|j_\pm|j,\Omega\rangle = \sqrt{(j\mp\Omega)(j\pm\Omega+1)} \quad . \tag{8}$$

Generally, H_c is non-diagonal, connecting bands that differ in Ω by one unit. However, as is well known, there is a diagonal contribution to bands with $\Omega = 1/2$. These rather simple basic equations will be used to treat all the cases of Coriolis coupling mentioned.

The ^{183}W case treated by Kerman involved only two bands with $\Omega = 3/2$ and $\Omega = 1/2$ and is shown in fig. 1. The initial bandhead energies, H_p', Kerman took as parameters, as he also did the initial $\hbar^2/2\mathcal{J}$ value for each band. In addition he took the $\Omega = 1/2$ band decoupling parameter to be adjustable. For a given value of these five parameters he could than calculate the initial energies of the levels in each band. For the parameters of his final fit, these are shown in fig. 1. Taking as a sixth parameter the value of $\langle\, \Omega = 3/2|j_+|\Omega = 1/2\,\rangle$, Kerman diagonalized the 2 χ 2 matrix for each spin,

giving the shifts shown in fig. 1. As is usual, the levels repel each other; levels of a given spin moving equal distances up and down. The experimental energies are listed at the edges of fig. 1, and it can be seen that the fit is indeed excellent. Kerman also considered some 20 M1 and E2 transition probabilities, achieving reasonable success at the expense of 5 additional parameters.

Subsequent work[4,5]) on ^{183}W has tended to confirm the basic principles of the Kerman analysis, though some problems have arisen. Rowe[4]) showed that various rotation-vibration ($\Delta K = \pm 2$) admixtures of the type found in even-even nuclei in the region of ^{183}W permitted one to obtain fits as good as Kerman's over a rather broad range of the parameters (though he obtained better fits for two particular sets of parameters). Brockmeier et al.[5]) later showed that including other Nilsson states could also significantly affect the fit. There are probably two conclusions to be drawn from this case: 1) there is clearly a significant Coriolis mixing of these bands; and 2) the details of this mixing are probably not very well determined due to the many parameters involved, and the possibility of contributions from a number of additional effects.

There are many other cases of moderate Coriolis mixing of two or three close-lying bands. The single-particle-transfer reactions have proved to be a powerful method for such studies since they give more direct evidence on the wave functions of the observed bands. However, I do not want to pursue such detailed analyses. The purpose of discussing this case was 1) to display the analysis of Coriolis effects in a simple case and 2) to show that even in a case of low $\hbar^2/2\mathcal{I}$, j and I, appreciable Coriolis effects occur. We will now go on to cases where the effects are larger and, at the same time, the

calculations are much less ambiguous.

2.2 ^{235}U

The unique-parity high-j orbitals within each major shell provide much the best cases to observe and understand large Coriolis effects in nuclei. It is essential to appreciate the reasons for this. The most obvious factor for these orbitals is that the Coriolis matrix elements increase approximately proportional to j for low values of Ω, as shown by eqs. (7) and (8). For the $j_{15/2}$ orbital, which is involved in ^{235}U, this implies matrix elements around 5 times larger than that found by Kerman for ^{183}W. This situation is typical for all the high-j orbitals, and leads immediately to the conclusion that any study of the largest Coriolis effects will involve these orbitals. The second fundamental reason for choosing these orbitals is that they are well separated from any other orbitals of the same parity, so that, to a very good approximation, j is pure. This can be verified from the Nilsson wave functions of: i) the $h_{11/2}$ orbital in the 50-82 shell, ii) the $i_{13/2}$ orbital in the 82-126 shell, and iii) the $j_{15/2}$ orbital in the shell beyond 126. This means not only that the above pure-j estimates for the Coriolis matrix elements are about correct, but also that all properties of the component states of these orbitals can be calculated with much higher than average reliability. To say it slightly differently, the properties of these states are not much affected by the small admixtures of other j-values, and hence not sensitive to the exact size of these admixtures. Yet another favorable aspect for the component states of a high-j orbital is that they will not Coriolis mix very much with states from other orbitals. This is both because of the pure j-value and because these other orbitals are at least one major shell removed in energy. We can summarize the properties of the high-j components as: 1) they comprise

a closed set of states whose Coriolis interactions among themselves are the largest possible; 2) they have very weak Coriolis interactions with states from other j-shells; and 3) their properties can be calculated with the highest reliability of any states in deformed nuclei.

One point about the reliability of calculated properties is illustrated in fig. 2. Here we show the components of an $h_{11/2}$ orbital as a function of deformation[3]). These components would be one of the closed sets of levels mentioned above. One sees that since they come from a given orbital ($h_{11/2}$) their relative energies are independent of the shell model parameters in the calculation, and depend only on the energy splitting of this orbital with deformation. This gives much more reliable relative energies than would otherwise be the case. To get the energies of the components one simply goes to the appropriate deformation, say $\beta = +0.275$, and reads off the energies at that deformation. A line on fig. 2 has been drawn to show these energies. In addition to β, one also needs to know the location of the Fermi surface, λ and the pairing gap, 2Δ, in order to calculate these energies as they might be expected to occur in a particular nucleus. The appropriate equation for the observed energy $E(\Omega)$ in terms of the eigenvalues from fig. 2, ε_Ω, is:

$$H_p \equiv E(\Omega) = \sqrt{(\varepsilon_\Omega - \lambda)^2 + \Delta^2} - \Delta \quad . \tag{9}$$

There is also a UV-factor[6]) to be included on the Coriolis matrix elements due to the pairing, but that is a small correction.

If we pick a Fermi surface near the $\Omega = 7/2$ level and apply eq. (9) to the eigenvalues of the $j_{15/2}$ Nilsson orbital at $\beta = 0.275$, the bandhead energies shown in fig. 3 result. We can then construct rotational bands on all these

bandheads according to eq. (6) - where H_p' is equated with $E(\Omega)$. The first few of these are shown for each band on fig. 3. The matrix elements, $\langle \Omega \pm 1 | j_\pm | \Omega \rangle$, as calculated from the Nilsson wave functions are also shown on fig. 3; and, by comparison with eq. (8), they can all be seen to be within 10% of the pure-j values. The procedure then is to pick out from each band the state of a particular spin, I, and diagonalize the resulting matrix. For the $j_{15/2}$ shell this will be an 8 x 8 matrix if $I \geq 15/2$, and smaller if $I < 15/2$.

Three things should be pointed out especially on fig. 3. First, a pattern much like this results from any high-j orbital. An $h_{11/2}$ orbital, for example, would have two fewer bands (13/2 and 15/2) and $\sim$ 30% lower matrix elements, but otherwise would be very similar. The second thing to note is that Coriolis effects are much bigger for the low Ω bands. Not only are the energy separations of the bands smaller here, but also the matrix elements are largest. Thus the very largest Coriolis effects will occur in low-Ω bands of high-j orbitals. Finally, the $\Omega = 1/2$ band has very anomalous spacings. Large decoupling factors always occur in these high-j orbitals, so this is a general feature. These anomalous spacings are transmitted to the $\Omega = 3/2$ band in the mixing process, and then on to the $\Omega = 5/2$ band in a second order process, etc. The resulting anomalous spacings in the higher-Ω bands are a very characteristic and important feature of the mixing we are describing here.

There are three favorable circumstances that make ^{235}U a very good case for studying such Coriolis calculations. The level scheme worked out from Coulomb excitation studies[7]) several years ago is shown in fig. 4. The first favorable feature is that many levels are observed in the $j_{15/2}$ component bands. Three bands, $\Omega = 5/2, 7/2, 9/2$, are seen and there are a total of 15 rotational spacings in these bands (bandhead energies are not included in the

fits in this case). A second advantage is that anomalous spacings coming from the mixing with the $\Omega = 1/2$ band are observed in both the $\Omega = 5/2$ and $7/2$ bands. This information alone tells some rather specific things about the Coriolis matrix elements. Finally the B(E2) values between the $\Omega = 7/2$ ground-band and both the $\Omega = 5/2$ and $\Omega = 9/2$ bands were determined. If one assumes that these B(E2) values result only from collective E2 transitions introduced by the mixing, then they give immediately the admixed amplitudes, and hence the Coriolis matrix elements involved. The assumption that the non-collective B(E2) values can be neglected is very likely to be essentially correct, but effects of 20% or so in the deduced mixing amplitudes cannot be excluded. Consideration of these features, and the other known E2 and M1 relative intensities, makes the ^{235}U case a real test for our description of these Coriolis effects.

I do not want to discuss the details of the calculations for ^{235}U, but only give an indication of the kind of results obtained. Figure 5 gives the results for the rotational energies where only one adjustable parameter was used. This plot is designed so that it gives a straight line for a rotational band if the band follows the equation,

$$E = E_0 + A\, I(I+1) + B\, I^2(I+1)^2 \quad , \qquad (10)$$

where the intercept of the line on fig. 5 would be A and the slope would be B. We use the plot because it can show the rotational energies on a sufficiently sensitive scale to see easily the anomalies in the $\Omega = 5/2$ and $7/2$ bands. In the calculation all bandhead energies and matrix elements were taken from the Nilsson wave functions except the matrix elements, $\langle 5/2|j_-|7/2\rangle$ and $\langle 7/2|j_-|9/2\rangle$, which were determined from the B(E2) values as described above.

The one parameter was $\hbar^2/2\mathcal{I}$, which comes into all the rotational band energies (eq. (6)) and matrix elements (eq. (7)) except the above two. The results clearly show the correct anomaly coming from the $\Omega = 1/2$ band into the $\Omega = 5/2$ and 7/2 bands. However the final effective $\hbar^2/2\mathcal{I}$ values for the $\Omega = 5/2$ and 9/2 bands are not correctly given.

The results of a three parameter fit are shown in fig. 6. Here the matrix elements, $\langle 5/2|j_-|7/2\rangle$ and $\langle 7/2|j_-|9/2\rangle$, were allowed to vary from the values indicated by the B(E2) values but their ratio was held constant, and the matrix element, $\langle 3/2|j_-|5/2\rangle$, could vary. The former of these went up by 20%, and the latter went down by 20%. The fit here is excellent (note the expansion of the ordinate scale). Also the known relative M1 and E2 transition probabilities were adequately given by wave functions from this fit. This fit is a very strong indication that we know how to make this kind of calculation. One minor puzzle comes out, whose solution is not at present understood. The matrix elements, $\langle 5/2|j_-|7/2\rangle$ and $\langle 7/2|j_-|9/2\rangle$, have values only about half as large as expected. This result comes from the measured B(E2) values almost completely unambiguously. This kind of effect on the Coriolis matrix elements near the Fermi surface has been observed in other similar cases, and is the outstanding remaining mystery in such calculations.

I have discussed the ^{235}U case in some detail for two reasons. First to show rather carefully how one treats such a j-shell, and secondly, to try to convince you that one <u>does</u> know how to make these calculations. I now want to go on to cases where the effects are bigger, but the data more meager.

2.3. Odd-A Er Isotopes

The calculated and experimental spectra of three odd-A Er isotopes[8] are shown in fig. 7. These data are for the lowest positive-parity band in these Er nuclei, and this band is clearly composed of heavily admixed components of the $i_{13/2}$ neutron orbital. One sees a reasonably normal $\Omega = 5/2$ band in ^{165}Er, large anomalies in ^{163}Er, and a band with some inverted level-orders in ^{161}Er. The calculations were very similar to those described for ^{235}U, except that here no data were available on higher bands. Nevertheless, the three parameter fits shown are impressive, and leave no doubt that the spectra are basically correctly interpreted. Figure 8 shows the rotational-energy plots like the ones just discussed for ^{235}U. The plot for ^{165}Er looks much like that of ^{235}U until one appreciates the ordinate scale. These effects are much larger than those in ^{235}U, and become still larger in ^{163}Er and ^{161}Er. In the latter case the inverted levels show up as negative points on such a plot. We can understand why these effects are big and get bigger with decreasing mass number. The rotational constant, $\hbar^2/2\mathcal{I}$, which comes into the Coriolis matrix elements (eq. (7)), is about twice as big here as in ^{235}U and is increasing with decreasing mass number in these Er nuclei.

2.4. Summary

In the Er nuclei the Coriolis effects are producing large distortions in the rotational bands. These effects can be calculated in some detail, as we have seen, but it now seems more useful to broaden our perspective on this problem rather than to study in detail such fits. There is no difficulty in solving eq. 4 for any deformation (except exactly zero) and it seems

essential to understand, in a general way, the nature of these solutions. If they contain some new regularities, then it is necessary to know just what these are so that they could be recognized if they occur in the Er (or other) level schemes. Along the same line it would be interesting to understand the physical process occuring in these distorted bands. These questions will be taken up in the next section, and in the beginning of section 4 we will return briefly to these Er nuclei and examine them from a somewhat different viewpoint.

3. Coriolis Effects in Nuclei with Small Deformations

Whether the Coriolis effects will be large or not in a particular case depends on the relationship of the rotational energy given by,

$$E_{rot} = \frac{\hbar^2}{2\mathcal{J}} I(I+1) \qquad (11)$$

and the energy separation between interacting states, that is the splitting between components of the j-shell of interest. We need to be able to estimate this relationship easily, and thus need to extend our mathematical framework a little further. That will be the first objective of the present section.

3.1. Calculations in Nuclei with Small Deformations

In cases where the Coriolis effects are large, we must use eq. (4) rather than the simplified eq. (6). There is some problem here, as the so called "recoil term", $\hbar^2/2\mathcal{J}\ [<\vec{j}^2> - \Omega^2]$, may already be empirically contained in the evaluations of H_p. However, the simple limiting solutions are not reached if the recoil term is not explicitly taken into account, so that in this section, at least, we will use the full eq. (4).

It would be convenient to be able to evaluate H_p in a simple way. This quantity can be expressed by giving the energy of the system as a function of Ω; that is, as a function of the orientation of j to the symmetry axis of the core. For a core with quadrupole deformation, the Nilsson calculations correspond to an evaluation of these energies as was mentioned (see fig. 2), but if the deformation, β, is not too large (i.e. if j is pure), then we can use the limiting approximation[6]):

$$\varepsilon_\Omega = E_0(n\ell j) + \frac{206\beta}{A^{1/3}} \left[\frac{3\Omega^2 - j(j+1)}{4j(j+1)} \right] \text{ MeV} \qquad (12)$$

The numerical coefficient, $206/A^{1/3}$, in eq. (12) gives reasonable agreement with the Nilsson, solutions for the $h_{11/2}$ and $i_{13/2}$ orbitals up to around $\beta = 0.3$, and a comparison of these two values for ε_Ω is given in fig. 2. Since we consider only a single j-shell, the $E_0(n\ell j)$ can be taken to be zero.

Using eqs. (4), (7), (8), (9), and (12) we could diagonalize a given j-shell for any value of I; however, there are four parameters to be fixed: $\hbar^2/2\mathcal{J}$, β, λ, and Δ. We can reduce these four parameters to two essential ones in the following way. There is a very general empirical relationship between $\hbar^2/2\mathcal{J}$ and β (as defined from the E2-transition lifetime) that essentially all even-even nuclei follow[9]). For the purpose of our survey we will use this relationship to eliminate one of these variables. This gives:

$$6(\hbar^2/2\mathcal{J}) \equiv E_{2+} \approx \frac{1225}{A^{7/3}\beta^2} \text{ MeV} \qquad (13)$$

We use β explicitly here only to interconnect $\hbar^2/2\mathcal{J}$ and ε_Ω, and one could take the point of view that eqs. (12) and (13) just define an empirical relationship between these quantities. That is to say, if we pick a value for the splitting of a given j-shell according to eq. (12), then eq. (13) does nothing more for us than pick a value of $\hbar^2/2\mathcal{J}$ that a real nucleus with the selected value for the splitting would be likely to have. However, some deformation is implicitly required for eq. (2) or (4) to have any physical meaning and it may well be that this is a physically real parameter. Of the remaining parameters, Δ is not very important and we take it always to be 0.8 MeV; so that there remain just two parameters β and λ.

We now have a simple set of equations that can be diagonalized for any values of I, β, and λ. Before we look at some of the detailed solutions, let us consider the limiting cases of large and small values for β. For large β ($\gtrsim 0.3$), the Coriolis effects are relatively unimportant since $\hbar^2/2\mathcal{J}$ is small (eq. (7)) and the different Ω components are widely separated (eq. (12)). This results in the usual strong-coupling limit of pure rotational bands with good Ω values. As we move toward smaller β, the Coriolis effects become more important and perturb this structure, mixing Ω values. This is the process we examined in section 2, and our model was shown to be reliable in this region. At the other limit, $\beta \approx 0$, $\hbar^2/2\mathcal{J}$ is large and the Ω separations are essentially zero, i.e. H_p is a constant (eqs. (9) and (12)), and although the diagonalization of eq. (4) appears complex, eq. (2) is now transparent, giving the result that the energies are just those due to the rotation of the core. It is, of course, true that the core of an odd-A nucleus is somewhat different from that of the adjacent even-even nucleus due to the blocked level, but we ignore that for the moment. In this limit there are states at each core energy having spin values that range from $|R - j|$ to $R + j$, and R is a good quantum number. This is just the spherically symmetric limit, and was discussed by Vogel[10]). Near this limit, eq. (4) gives results identical to those of a weak-coupling model[11]) with (apart from the pairing effects) a pure quadrupole-quadrupole particle-core interaction. The relevant feature of such a model is that the core state is split into a multiplet centered on the core energy, but not otherwise dependent on that energy nor on any other property of the core. Thus even though the pure-rotational core energies given by eq. (4) are not realistic for this region, the splitting of the core levels will be reasonable, if the

real interaction is quadrupole-quadrupole (plus the pairing effects) and if our estimate of the effective quadrupole strength (eqs. (12) and (13)) is about right. Thus we will also examine eq. (4) in this region of small β-values, but we should at best only take seriously the positions of the various levels relative to the position of the related core state.

We now want to examine the solutions to eq. (4) as a function of β and λ. Our first objective will be to show that in the heavier elements a study of the interesting new physical situations really does not require any variation of λ. The argument can be made with reference to fig. 2. For very large Coriolis effects, $\hbar^2/2\mathcal{J}$ must be large, which means β must be small (eq. (13)). However, once we are past the region of Sn, β is only small at the beginning or end of major shells. In the middle of major shells one finds regions of large deformation--the rare-earth and actinide regions. Since the unique-parity high-j orbitals lie more or less in the middle of the major shell it follows that regions of very large Coriolis effects occur only if λ is quite low or quite high in this orbital. When λ is in the middle, the nuclei have large deformations, and the Coriolis effects are minor perturbations and already basically understood. Furthermore, it can be seen from fig. 2 and eq. (9) that for pure-j wave functions the regions of low and high λ are identical if one just interchanges the prolate and the oblate side. This is not exactly true for the Nilsson solutions (solid lines), but is a rather good approximation in that case. Thus the interesting new situations can be studied using only a single value for λ, and we have chosen a value corresponding to the bottom of fig. 2, -4.5 MeV. This is below the entire orbital for $|\beta| \lesssim 0.3$. For very high λ values (top of fig. 2), we then only interchange the prolate and oblate sides. For comparison with particular cases, it is

clear one should use λ values as close to reality as possible, but the present single choice will show all the new effects. Note that for our choice of λ, low Ω values, and hence large Coriolis effects, occur on the prolate side, and high Ω values, with smaller Coriolis effects, on the oblate side.

The solutions of eq. (4) for the $h_{11/2}$ orbital with $\lambda = -4.5$ MeV (fig. 2) are shown in fig. 9. The ordinate here is the eigenvalue for spin, I, minus the lowest I = 11/2 eigenvalue, divided by E_{2+}. Only the yrast levels (lowest energy for each I) are plotted except for the second lowest I = 11/2 state. The spin sequence I = j, j + 2, j + 4, . . . has been darkened to help make these levels stand out. At $\beta = 0$, the degenerate solutions having the core energy values are apparent. A region of possible application for a weak-coupling model is seen between $-0.1 \leq \beta \leq 0.1$, where the splitting of the core multiplets is less than the core energy separations. Outside this region such a model could not be expected to apply. On the oblate side, where the Coriolis effects are weak (due to the large separations between Ω components, eq. (12), and the small matrix elements, eq. (8)), a recognizable $\Omega = 11/2$ rotational band develops very quickly. The order of levels is correct all the way from $\beta = 0$, and by $\beta = -0.15$ the band spacings are becoming rather close to the rotational ones. This is clearly what should be expected, since the $\Omega = 11/2$ level is nearest to λ, and the Coriolis effects are weak on this side.

On the prolate side the situation is more interesting. The $\Omega = 1/2$ level is nearest to λ over the range of β values plotted, so that the lowest levels are tending toward the energies for such a band. But the Coriolis effects are large on this side, and even at $\beta = 0.3$ the levels are rather far from those of an $\Omega = 1/2$ band. The outstanding feature on this side is the

coincidence of the energies of the "favored yrast" states ($I = j, j + 2, j + 4, \ldots$) with those of the core states for essentially all β-values. Note that the separations between these levels are very small compared to what one would expect for any normal rotational band--as may be judged by those at the same β on the oblate side of fig. 9. These levels lie very low in energy for their spin value; thus the name, favored. The favored/yrast band of high-spin states is important because there seems to be experimental evidence accumulating that it occurs frequently in odd-A nuclei. In the next subsection we will examine the physical effect responsible for this behavior. A final comment about fig. 9: if $j - 11/2$ is added to all spin values, then it would apply approximately to any high j-shell. Thus the process we are interested in, is a very general one.

3.2. The Physical Effect

The physical picture for the oblate side of fig. 9 is rather simple. Here the Coriolis effects are weak and the particle follows the core rotational motion even for rather small values of β, and thus the usual strong-coupling description applies. At, or very near, the center of fig. 9, where β is very small, the particle does not feel the core rotational motion at all since the coupling to the deformation is small and the rotational frequency is large. This is expressed by the degeneracy of all the orientations of the particle angular momentum relative to that of the core. In this region the rotational energies are very high (eq. (13)) and the model we are discussing is not likely to be applicable. A guess as to the limit for applicability of the present model might be something like $|\beta| \gtrsim 0.1$ ($E_{2+} < 1$ MeV). The interesting region

occurs on the prolate side of fig. 9 where the particle is neither completely decoupled from the rotation nor strongly coupled to it. We will be particularly interested in the favored yrast band on this side because so far most of the experimental data available are for such levels. In order to make up the I value, these levels must have R nearly parallel to j and we saw in fig. 9 that they coincide with the core energies out to very large β values. These are the properties that seem to be important to understand.

To demonstrate the physical effect involved for these states, we need only consider qualitatively a particle coupled to a rotating core. The principal influence of the rotation on this coupling can be expressed by introducing the Coriolis effects, and these depend essentially on the Coriolis force, proportional to $\vec{R} \times \vec{j}$, where $\vec{R}$ and $\vec{j}$ are the core and particle angular momenta. But for those states where $\vec{R}$ is coupled almost parallel to $\vec{j}$, achieving the maximum I, $\vec{R} \times \vec{j}$ is nearly zero. Thus the rotation has little effect on the coupling of the particle to the core for this orientation of the two, and the energy changes of the system just reflect the core energy changes. This is the reason we refer to such a band of levels as rotation-particle decoupled, or just "decoupled". We will use this name more or less interchangeably with "favored yrast"; however, the former name implies this interpretation, whereas the latter does not imply any particular interpretation.

This argument can be illustrated using fig. 10, where we show a wheel (representing the high-j particle) on a turntable (a blurred-out rotating core where the axis of the core lies in the plane of the turntable). In fig. 10a the angular momenta of the two are perpendicular, producing a maximum Coriolis force ($\vec{R} \times \vec{j}$). Thus the wheel (particle) "feels" the rotation of the turntable

(core). The resultant force is in a direction which tends to produce the configuration in fig. 10b, where the two angular momenta are parallel and the Coriolis force on the wheel thus vanishes. In the orientation represented in fig. 10b, the wheel can no longer feel, or interact with, the rotation of the turntable. They are decoupled.

Another illustration of this point is shown in fig. 11. In the upper portion the usual strong-coupling scheme is represented. Here j precesses around the nuclear symmetry (z) axis with constant projection Ω. A mixture of R values is required to construct a good total angular momentum, I. If this state lies lowest in energy it is because the energy advantage in the state Ω is so great that R values larger than the minimum one can be afforded. There are really two coupling schemes represented in the lower part of fig. 11. In the first, R is a good quantum number of the system, and its direction is specified by the fact that it has zero projection on the symmetry axis. It is shown in fig. 11 as being parallel with the rotational axis (or x-axis) which is similar (especially at high spin values). This scheme corresponds to the spherical limit, which was discussed in some detail above, and requires a mixture of Ω values, as indicated. The third scheme is a very interesting one and corresponds to sharp projections of j on the rotational axis. The decoupled states are the ones where this projection is a maximum, 11/2 for the $h_{11/2}$ orbital we have been discussing. Mottelson[12]) has pointed out that this is a simple coupling scheme which might apply to all the levels at moderately large rotational frequencies. In fact, around $\beta = +0.2$ on fig. 9, the solutions to eq. (4) do correspond to this coupling scheme with remarkable accuracy. For example, at $\beta = 0.2$ the lowest I = 11/2 solution "contains" (square of the

of the overlap integral) 98% of the state having a projection of 11/2 on the rotation axis; whereas it contains only 46% of the R = 0 state and 55% of the Ω = 1/2 state. Thus, it is much the best represented in the first of these three coupling schemes. The present scheme and the one with sharp R values are similar, and become virtually identical for large spin values, but the solutions to eq. (4) around β = +0.2 on fig. 9 clearly correspond much more accurately with the present scheme. Both schemes give very nearly the R(R+1) relative energy spacings of the core for the favored yrast states, and this can perhaps help explain the very flat behavior with energy of these states in this region of deformation.

3.3. Odd-A La Nuclei

Gamma-ray studies[13]) on the light odd-A La nuclei following Sn(^{14}N,3n)La reactions revealed a cascade of stretched E2 transitions, in each La nucleus, having energies very close to the values for the Ba nuclei with one less proton. Studies of the Ba(^{4}He,t)La reaction[14]) indicated that this cascade was based on an 11/2 state. Fig. 12 shows the energies of these cascades compared with the even-even Ba nuclei. The correspondence is remarkable, and provided the main incentive for studying eq. (4) at low β values[15]). If one used the even-even Ce nuclei for comparison instead of the Ba ones, the correspondence would be rather similar, as the even-even energies are not changing very rapidly with proton number in this region. It has been suggested[15]) that these states comprise the decoupled band based on the $h_{11/2}$ orbital. Unfortunately there is no information on the location of the other negative parity states in the La nuclei.

Qualitative evidence on the spectroscopic factors from the (^{4}He,t) reaction tends to support this interpretation. In the deformed coupling scheme, transfer of a particle from the ground state of an even-even nucleus to an odd-A one populates states with R = 0. Normally the R = 0 state is distributed equally over the (2j+1)/2 component bands of a j-orbital. However the Coriolis mixing, which we are discussing, builds up the R = 0 amplitude in the lowest I = j state, until it is a pure R = 0 state at the spherical limit. This behavior is consistent with the observed spectroscopic factors in the La nuclei, but a quantitative analysis of the data has not yet been made.

In fig. 13 the results of a calculation are shown which look very much like those shown in the prolate portion of fig. 9. Actually, in fig. 13 the Fermi surface is kept exactly at the $\Omega = 1/2$ level at all deformations. This is about 2.5 MeV different from fig. 9 at $\beta \approx 0.2$, and just shows the insensitivity of the results to the exact location of the Fermi surface, provided it is below the entire orbital. In the La nuclei, λ is probably somewhere between these two values. If β is fixed at 0.25, fig. 14 shows the effect of varying λ. The relative spacings of the favored yrast states are not very much affected until λ gets up to about the $\Omega = 5/2$ level, then they begin to rise sharply toward their rotational values. Only when λ reaches the 9/2 level or above, do the spectra have reasonably good rotational bands for this β value.

3.4. The Au Region

Before discussing the nuclei in the Au region, we should add one more aspect to our mathematical framework. One of the serious drawbacks of eq. (2) is that the core spacings are always those of a rigid rotor, i.e. they follow

eq. (11). It is easy to relax that requirement somewhat if we use instead of eq. (2):

$$H = H_p + \hbar^2/2\mathcal{J}\,[\vec{R}^2 + B\vec{R}^4 + C\vec{R}^6] \quad , \tag{14}$$

where B and C can be varied to give approximate fits to the relevant even-even nuclei. Small effects due to such things as centrifugal stretching, and perhaps quadrupole vibrations of the core can be included in this way. Although more complex mathematically, eq. (14) can be diagonalized in just the same way as eq. (2).

For the nuclei in the Au region, we will fix β and λ in a particular case, so that there remain no adjustable parameters. We fix β by averaging the value for the two adjacent even-even nuclei. For this value of β, λ is fixed at or near the level corresponding to the correct number of particles according to the Nilsson diagram. Thus for each odd-A case we calculate two spectra, corresponding to either a prolate or an oblate shape for the nucleus. Within the framework of our model, these are unique predictions for each case.

We will now discuss briefly our conclusions about this region of the periodic table. We will first consider the $h_{9/2}$ and $h_{11/2}$ proton orbitals. A portion of the Nilsson diagram for protons is shown in fig. 15, which contains particularly these orbitals. The Tl and Au nuclei have λ values around 3 or 4 MeV on this figure, and this lies completely below the $h_{9/2}$ orbital for $|\beta| \lesssim 0.2$. Thus the situation described in constructing fig. 9 is applicable, and we need only change j from 11/2 to 9/2. The calculation for the correct j and λ is shown in fig. 16. The similarity to fig. 9 is apparent. For the Tl nuclei we use a $|\beta|$ value of 0.11, which is taken from the Hg nuclei. Since

the odd proton is, in this case, lifted out of the 50-82 shell, we have not averaged the Pb and Hg values. One set of dots in fig. 16 shows the location of the levels of ^{199}Tl, taken as representative of the lighter Tl isotopes and normalized to the lowest I = j calculated level. The rotational-bandlike character of these levels has previously[16]) been noted, and, according to fig. 16, immediately requires an oblate shape for these states. This, also, was previously proposed. The calculated energy spacings are considerably wider than those observed, but this is largely corrected if one diagonalizes eq. (14), dashed lines in fig. 14, instead of eq. (2), with B and C adjusted to approximate the lowest few ^{198}Hg levels. A more detailed comparison of these levels is shown in fig. 17. It seems that the prediction of: (a) rotational bands in Tl nuclei; (b) the approximate $\hbar^2/2\mathcal{J}$ value of these bands; and (c) the sign and rough magnitude of the deviations from a purely rotational spectrum, are rather convincing for a calculation with no adjustable parameters. To show that our calculations go over into the region of large deformation in reasonable fashion, we have also indicated in fig. 16 the predictions for ^{179}Re, where β is taken from ^{180}W and ^{178}Os, together with the observed states[17]). A lower λ-value should be used for Re, but this would make very little difference here. Again the order of levels is correct, as is the approximate spacing of these levels. In this case the prolate shape requires a spectrum between the decoupled type and one having $\Omega = 1/2$. Our interpretation of these levels is consistent with that previously made[17]).

The situation for the $h_{11/2}$ orbital is shown in fig. 18, and is quite similar to that of fig. 9, except that the oblate and prolate sides are reversed. This reversal is seen in fig. 15 to be a result of the fact that λ is now above

the $h_{11/2}$ orbital rather than below it. The predicted position of ^{195}Au is indicated, with β taken from ^{196}Hg and ^{194}Pt, and the experimental points are again shown as dots[18]). In this case an oblate shape is clearly indicated by the decoupled-type Au spectrum. Again the order of levels and spacings are surprisingly well given, and are improved somewhat by the use of eq. (14), as the more detailed comparison of fig. 19 shows. However, the reversal of the of the I = 13/2 and 9/2 states does not come about easily, as far as we can see, for purely oblate shapes. Since λ is not entirely above the $h_{11/2}$ orbital at $\beta \sim 0.2$, we readjusted it for ^{179}Re as shown in the lower portion of fig. 18; however the differences are really not very large. The previously identified $\Omega = 9/2$ band in ^{179}Re is shown to be in rather good agreement with the calculations for a prolate shape, although the moment of inertia of the band is underestimated. This is not surprising since it always happens for these high-j orbitals in well-deformed nuclei if the Coriolis strength is not reduced somewhat compared with the a priori estimates.

Our recent experimental results[19]) on the high-spin states in the odd-A Hg nuclei also seem to indicate the presence of decoupled bands. A series of two or three stretched E2 transitions were observed in ^{189,195,197,199}Hg whose energies approximated those of the adjacent even-even nuclei. In some cases it could be shown that these cascades terminated in the well-known $i_{13/2}$ isomers. This is precisely what one would expect from the $i_{13/2}$ orbital around $\beta = 0.1$ according to the present calculations. Thus in Tl, Hg, and Au, the high-j orbitals seem consistently to occur with oblate shapes, having either the decoupled or near-rotational type of spectra.

3.5. Summary

It seems to us that the model of a particle coupled to a non-spherical rotational core works very well for the high-j orbitals in the region just below lead and also in the La region. Most of the data are on the favored yrast states, but some data exist on lower spin states. It is not very clear at present just what this agreement means. Three possibilities occur to us: (1) the least general would be that the picture is valid only for states of the maximum I, that is for the high-spin yrast states which are generally the ones observed experimentally; (2) it might be that out of some more general model there does emerge a set of core states that look like rotational states and couple as we describe, but other core states would also be present giving rise to additional states beyond those we calculate; and (3) the rotational core states may be the only low-lying ones and thus, for the high-j orbitals, our calculations are both valid (approximately) and complete. The lower-spin states in Au suggest that perhaps more than (1) is true, but much work remains to decide just where the truth lies. For lower-j orbitals the situation is even less clear. Extensive calculations have been made by Malik and Scholz[20]) in the mass region, A = 25-80. The results of such attempts are generally encouraging although the data were nowhere sufficient to provide an altogether convincing picture. The high-spin yrast states have not been studied there, and so far they are the only ones for which there is extensive data that support the model in a very specific way.

Even within the model there are a number of approximations. It is fairly easy to show that some, such as the assumption of pure j-values are not serious. The three that seem to us most likely to be serious are:

(a) the use of a perfect rotor Hamiltonian for the core (eq. (14) represents only a very limited attempt to relax this); (b) the neglect of the effect of the odd particle on the core parameters; and (c) the restriction of the core to axially symmetric shapes. We cannot estimate very specifically how serious any of these are likely to be. Thus, the model we discuss seems to have some very promising aspects, but much work remains to be done; first to understand the model more completely, and second to understand the limits of its applicability to nuclei in the region of small deformations.

4. Coriolis Effects in Even-Even Nuclei

There are some indications that the Coriolis effects in the high-j orbitals also play an important role in the high spin states of even-even nuclei. It is not difficult to see that this might be the case. If one considers the question of which two-quasi particle (2qp) states of an even-even nucleus are likely to lie lowest in energy at spin 20, then the maximum Coriolis energy given by eq. (1) becomes an important factor. If both particles are in a high-j orbital, then eq. (1) applies, approximately, for each particle, and a total energy lowering of 5 MeV is reasonable to expect for $i_{13/2}$ particles. It seems clear that such an energy might be decisive in establishing these states as the ones that are systematically lowest at such spin values. Later in this section we will try to show in some detail why an understanding of the lowest 2qp states may be important for these spin values. It is clear that we do not yet fully understand the yrast states in even-even nuclei around spin 20; however, the present discussion, supported by detailed calculations, suggests that they could well be strongly influenced by Coriolis effects.

The present section will be divided into three parts. First I will summarize the experimental data bearing on high-spin states in even-even nuclei. Second, I will try to show, using odd-A nuclei in the Er region, that a high-j particle in this region would tend to be largely decoupled at the spin values involved. Finally, I will discuss the results of our two-particle Coriolis calculations and compare them with some other interpretations.

4.1. Experimental Data and Interpretation

Of the two types of data bearing on the question of very high spin states in even-even nuclei, the older one has to do with the de-excitation cascade in

product nuclei following heavy-ion compound-nucleus (HI,xn) reactions. This information has recently been summarized and some of its implications about the nature of such high-spin states discussed[21]). The gamma-ray spectra from these product nuclei almost invariably consist of a set of discrete lines on a continuous background. In rotational and vibrational nuclei the lines correspond to the transitions in the ground-state collective band (gsb)[†], and represent the last steps of the de-excitation. Thus the gamma-ray transitions between the high-spin states are in the continuous background. Up to now very few direct studies of this continuum have been made, so that the information about the high-spin states is based on observations of the transitions between lower-spin states--i.e., the discrete lines. The following points, made in ref. [21]), are relevant to the present discussion: a) the maximum spin observed in the gsb ranges from around 16 for rotors to around 6 for vibrators, and this maximum is characteristic of the particular nucleus (not of the reaction); b) however, when heavy ions are used to produce the compound nucleus (bringing in high angular momentum) then the gsb is fed <u>mostly</u> at or near the highest observed level, whereas with light projectiles the feeding pattern is related to the distribution of angular momentum brought in by the projectile; c) the mean time interval between the reaction and population of the gsb in rotational nuclei is very short, $\lesssim$ 10 psec; and d) very high-spin isomers--I $\gtrsim$ 20 $\hbar$--have never been observed. It should be emphasized that these are features observed in (especially) rotational and vibrational nuclei, and would not apply, without modification or qualification, to closed-shell or near-closed-shell nuclei.

[†]The gsb refers to the collective band based on the ground-state configuration of a particular nucleus. For the even-even nuclei considered here, this is a completely paired configuration--zero quasi-particles--, and the levels of this band are the yrast levels at low spin values.

To understand these four points, the de-excitation was described in ref.[21]) as consisting of three cascades, whose existence had been previously proposed by Grover[22]) based on numerical studies of the process. These are schematically indicated in fig. 20. Since the initial energy (20 MeV) and level density are high, a statistical cascade (I) consisting mainly of high-energy dipole transitions is expected to occur first. This carries off around half the excitation energy but very little angular momentum and is terminated by coming into a region where the level density is no longer high. This region is located just above the yrast level and would be $\approx$ 10 MeV for I $\approx$ 35 in the above example. At this point the cascade is forced to begin carrying off angular momentum and follows, more or less closely, the yrast levels down in spin. This is called the yrast cascade (II). At some spin the yrast levels become those of the gsb and an energy gap develops between these levels and others of the same spin. At this point the population shifts rather suddenly into the gsb through which it cascades (III) to the ground state. fig. 20, which is taken from ref. [21]), shows the essential features of these three cascades. For lighter projectiles, where less angular momentum is brought in, the length of the yrast cascade shortens, until it is essentially absent in reactions induced by ^{4}He.

Two interesting conclusions were drawn in ref.[21]) about this de-excitation. First, the very short feeding times and absence of isomeric states with high spin indicate that energies in the high-spin yrast region must be very smooth and the transitions between these levels must be enhanced over the single-particle value if they are E2. (Other choices for the predominant multipolarity turn out to be much more difficult to explain.) Furthermore, to avoid the generation of discrete lines in this region, the population must be spread over several ($\gtrsim$ 5) levels. It was suggested[21]) that the presence

of rotational bands admixed by the strong Coriolis force present at these high spins might produce such features. Mottelson[23]) has pointed out that the spectrum of an asymmetric rotor is a particularly simple one fulfilling these requirements of the yrast cascade, but a model for the de-excitation based on this suggestion has not been published. The second conclusion of ref. [21]) was that the feeding point of the gsb was near its intersection with other levels. No other way could be found to explain the population patterns. This intersection implies a major change in the nature of the yrast levels above this spin value.

Very recently A. Johnson et al.[24]) have found some irregularities in the rotational energy spacings of rare-earth nuclei just in the region of spin where they are populated heavily in these (HI,xn) reactions. These are shown in fig. 21, where the moment of inertia for several rare-earth nuclei is plotted against the square of the rotational frequency. The irregularity, called backbending or S-shapes, is apparent. This seems to be a fairly general behavior in this region of the periodic table, and it lends very strong support to the previous proposal that a major change is occurring in the yrast levels near this point. Johnson et al. suggest that this change is due to the phase transition associated with the loss of pairing correlations predicted by Mottelson and Valatin[25]) to occur at around this spin value. I would like to point out that a simple, very general interpretation of this behavior is that the ground band is intersecting some other level or levels. This interpretation probably can be equivalent to that of Mottelson and Valatin if the band intersected is one with no pairing correlations. Since this point is an important one for the present arguments, I will discuss it briefly.

In the general case where the ground band intersects another band, the features of the rotational spacings can be reasonably well characterized. Fig. 22 shows the simplified situation of two bands with constant--but different--moments of inertia around their intersection point at I_c (16 in this case). We want to follow the lowest band, and if there is no interaction between the bands we simply change suddenly from one to the other at I_c. When plotted as $\mathcal{J}$ vs. ω^2, this makes a discontinuity as shown by the dashed line in Fig. 23. This discontinuity causes lower values of ω^2 above I_c if $\mathcal{J}_2/\mathcal{J}_1 > (I_c + 2)/I_c$. This might generally be the case around I = 20 since $(I_c + 2)/I_c$ is then only ~ 1.1. As an interaction is introduced between the bands, the discontinuity is rounded, first into an S-shaped curve like A in Fig. 23, and then with increasing interaction, like B and finally C. This range covers the observed behaviors, those of Johnson et al. being of the S-shaped variety (A or B in Fig. 23), whereas most previously measured ones appear to be more like C. Thus, for intersecting bands, the occurrence of S-shaped curves depends on two factors: (1) the difference between the effective moments of inertia of the two bands at their intersection point, which determines the transition to be made, and (2) the strength of the interaction between the bands which determines how sharply this transition is made.

To summarize, the above discussion shows that there is good evidence for a major change in the nature of the yrast levels of rare-earth nuclei somewhat below I = 20, and furthermore, that at higher spin values a new very regular structure develops. Both types of information on these high spin levels have been shown to be consistent with an intersection of the ground band with another band (or bands). The interesting physics is in what kind of a band is

intersecting the ground band, and so far two different answers have been given. The Mottelson-Valatin argument would suggest that a band with no pairing correlations is the one lying lowest after this intersection. We have suggested[26] that the intersecting band may be a 2qp band composed of particles in high-j orbitals (due to the enormous Coriolis energies available to these bands at such high spin values). In the next subsection I will try to show that in the Er region, at the spin values where these S-shaped curves are observed, it is reasonable to suppose that particles in the $i_{13/2}$ orbital would be decoupled. We will then go on in section 4.3 to see what such decoupling means in an even-even nucleus.

4.2. Decoupling in the Er Region

The decoupled state, described in section 3, is one where the particle angular momentum, j, is parallel to the core angular momentum, R. In this situation there is no Coriolis coupling between the particle and the core. Thus, if a core is rotated at different frequencies, the energy changes of the system are just the differences in core rotational energy. That is, the energy spacings of the decoupled system are just those of the related even-even core. We saw this behavior in the odd-A La, Au, and Hg nuclei in section 3. We now want to examine the odd-A Er nuclei to see the kind of behavior to be expected in that region.

The high-j orbital involved in the odd-A Er nuclei is the $i_{13/2}$ neutron orbital. Fig. 24 shows the rotational energies, in units of $\hbar^2/2\mathfrak{I}$, expected in bands based on this orbital for the strongly-coupled and the decoupled schemes. On the left is the usual rotational-band picture with the correct relative

energies. If Ω is less than 13/2, then there will be levels lower than the one shown at I = 13/2, but the relative energies of the levels shown is independent of that. The I = 17/2 to I = 13/2 energy difference is $32\frac{\hbar^2}{2\mathcal{J}}$. On the right side of fig. 24 are shown the favored yrast levels of the decoupled scheme. Here the I = 17/2 to I = 13/2 energy difference is just the even-even I = 2 to I = 0 energy difference, namely $6\frac{\hbar^2}{2\mathcal{J}}$. Thus, it is easy to see that a measure of this particular energy difference, relative to that of the adjacent even-even nuclei, gives a very simple and direct measure of how decoupled the $i_{13/2}$ particle is.

In fig. 25 I have made a plot of the 17/2 - 13/2 energy difference divided by E_{2+} (as defined to be the average of the two adjacent even-even nuclei) as a function of neutron number for nuclei in the region of erbium. The coupled and the decoupled limits, discussed above, are shown, and the solid points represent the known nuclei. It is apparent that on the right side of fig. 25 the points are about midway between the two limits; whereas, on the left side the nuclei are essentially completely decoupled. Tentative data on ^{155}Er indicates that it, too, is at the decoupled limit for these spins. The open points show the effect of going to higher spin values in the Er nuclei. The second highest point represents $(E_{21/2} - E_{17/2})/(E_{4+} - E_{2+})$, and so on (except in the case of ^{157}Er, where the order is inverted). At higher spin values the points are clearly nearer the decoupled limit; so that, by the time one is four units of spin above the minimum, all the Er nuclei are within 20% of the decoupled limit. I should point out that the coupled limit on fig. 25 moves down as the spins increase, so that the approach to the decoupled line is not quite so impressive as it appears on the figure. Nevertheless, the

three heavier Er nuclei move down rather strongly at the higher spins even if one plots as a percentage of the difference between the limits. It is clear why the higher spin values and/or the lighter Er nuclei approach the decoupled limit. Eq. (1) shows that the Coriolis effects go up with both spin and $\hbar^2/2\mathcal{J}$. The increase in $\hbar^2/2\mathcal{J}$ is rather sharp as one moves toward lower neutron number in this region.

The relevance of this discussion to the even-even nuclei is as follows. It is possible to show, in lowest order, that if you couple two high-j particles to their maximum J, (2j - 1) then the degree of decoupling of the two particles at spin I = J should be similar to that of one particle at spin, I = j. This would say that in a 2qp state, based on $i_{13/2}$ particles, with I = J = 12, we might expect the amount of decoupling indicated for the solid points in fig. 25; that is, they should be decoupled around N $\approx$ 90, but intermediate at N $\approx$ 98. However, going a few units of spin higher than 12 should produce essentially complete decoupling for all the nuclei in this region. This simple and direct evidence enables us to make predictions about the energy of the 2qp states which are independent of the detailed calculations we would otherwise have to use. (Note, however, that the calculations describe these odd-A Er nuclei rather well, fig. 7.) The calculations have been done for the even-even cases[26]), and give the same result--that by I = 16 or so all these cases should be essentially decoupled--but I believe that fig. 25 is perhaps a more convincing argument for this. We now want to see just what this means for an even-even nucleus.

4.3. The Even-Even Nuclei

In fig. 26 I have drawn simple estimates for the energies of three bands in an even-even nucleus. The solid line is the ground-state band with a constant value of $\hbar^2/2\mathfrak{J}$ of 15 keV. The dashed line is the estimated curve for the decoupled case. Here I have estimated that it takes 1.5 MeV to remove a pair of $i_{13/2}$ particles from the pairing correlations. Then it takes some additional recoil energy (eq. (4), see also section 3.1) to decouple the particles. This can be estimated to be about 1 MeV. Thus by expending about 2.5 MeV we have two $i_{13/2}$ particles that can be oriented in any direction to give any spin value up to I = 12 without further expenditure of energy. This is indicated by the flat portion of the dashed line in fig. 26 out to I = 12. Beyond I = 12 additional angular momentum can be added by rotating the core with angular momentum, $2\hbar$, $4\hbar$, etc., and I have taken the ground-band value of $\hbar^2/2\mathfrak{J}$ to extend the decoupled curve in this region. On this naive picture it can be seen that the ground band intersects the decoupled band around I = 12, and we have proposed that this is the intersection the experimental data have indicated. A failure of the decoupled band to decouple completely will raise that curve in fig. 26, and produce an intersection at higher spin values, in better agreement with the data. The dotted curve in fig. 26 represents the Mottelson-Valatin case. Here I assumed 2.5 MeV was required to destroy all the pairing correlations in the nucleus, and then rotation could occur with the rigid body moment of inertia-- $\sim$7 keV. This line also intersects the ground band and could produce the experimental intersection. Fig. 26 is quite schematic and certainly one should not try to estimate from it which intersection occurs at lower I values. In fact, probably neither of these two upper bands exist at low spin values as a discrete band. Nevertheless, fig. 26 can give an overall impression of the situation I will be discussing.

I will describe briefly the mathematics used in the even-even case so that one has some idea of what is involved. In fig. 27 the coupling scheme is indicated, where two particles with angular momentum, j, couple to a total J, which then couples with R to give I. The projections of the two j values on the symmetry axis are labeled Ω_1 and Ω_2. Fig. 28 shows the lowest few $i_{13/2}$ component levels, in a situation where λ is between the 3/2 and 5/2 components. The left side shows the main configuration of the even-even ground state, and the right side shows a 2qp state of the type we are discussing. This state has K = 1, and is connected to the ground state by a large Coriolis matrix element of the type we have discussed. If we consider only the lowest three levels in fig. 28, Ω = 1/2, 3/2, and 5/2, and generate all the 2qp states possible, then the resulting spectrum is shown in fig. 29. The Fermi surface was assumed to be between the Ω = 3/2 and 5/2 states in this figure. All the non-zero Coriolis matrix elements have been shown as lines between the connected states. One sees that with only three Ω values a complicated pattern develops. However, this system can be diagonalized in just the previous way; and, in fact, the full $i_{13/2}$ orbital has been studied[26]), including all possible (49) 2qp states. Also the lowest 4 Ω-levels have been used to construct all possible 2qp and 4qp states, and this system was also studied; so that, we have a reasonable idea what to expect from the calculations in these even-even cases. It should perhaps be noted that eq. (4) applies to such a system if $\vec{J}$ is substituted for $\vec{j}$, and one needs only the additional relationship:

$$\vec{J} = \vec{j}(1) + \vec{j}(2) \quad . \tag{15}$$

The reliability of these 2qp calculations is not expected to be much worse than that of the one-particle case (section 2).

The lowest two solutions of the even-even case (with the Fermi surface located as in fig. 28) are shown in fig. 30 for three different β values: $\beta = 0.3$, solid lines; $\beta = 0.2$, dashed lines; and $\beta = 0.1$, dotted lines. The $\beta = 0.1$ case should not be taken too seriously, since the model is not so likely to apply here, but it was included to show the trends. In all three cases the 2qp (largely decoupled) band starts out around 2.5 MeV, is rather flat out to $I \approx 12$, and then goes up with about the ground-band $\hbar^2/2\mathcal{J}$ value. In all cases it crosses the ground band; however, for the $\beta = 0.3$ case the crossing is very smooth, and not so apparent since the levels repel each other and do not get closer together than about 1 MeV. Nevertheless, plotted on an $\mathcal{J}$ *vs.* ω^2 plot, the ground-band line in fig. 30 does have a typical "kink" in it (not quite an S-shape). The earlier intersections in the $\beta = 0.2$ and 0.1 cases are caused mainly by the wider ground-band spacings which are just due to the larger $\hbar^2/2\mathcal{J}$ value used. One sees that the kink, which was not even visible for $\beta = 0.3$, becomes very large for $\beta = 0.2$, and pathological (though probably not at all reliable) for $\beta = 0.1$. The numbers on fig. 30 are the calculated total populations passing through each state. These are obtained from the (collective) B(E2) values and energies obtained from the calculations, where equal initial population was assumed in all (50) levels at $I = 30$. The calculated populations look very much like the experimental ones, in general. The feeding in all cases comes in around the intersection point. The reason for this is easy to understand, and will be discussed briefly, since it is a simple and very general argument.

In fig. 31, we indicate the lowest few solutions from the matrix diagonalization for spin I, and label them m = 1, 2, etc., according to energy. The

same is done for spin I + 2, with n as the labeling index. The Coriolis interaction varies slowly with I, for large I, so that the main difference between the matrices for I and I + 2 is that the initial energies of each state differs by the rotational energy--as in eq. (4) or (6). Thus the main difference in the solutions will be this difference of a rotational energy, which is quite smooth with I. To higher order, if the interaction is increasing with I--the Coriolis interaction is approximately linear with I--then in the energy region of interest the I + 2 states will be lowered with respect to the I states, and the mixed band will be compressed in energy over the input bands. Since the difference between the I and I + 2 matrices is small, the lowest solution from I will have a wave function similar to that of the lowest solution of I + 2, etc.

We now consider the B(E2) values between the states indicated in fig. 31. The wave functions for a given solution, $|IM,m\rangle$, can be written:

$$|IM,m\rangle = \sum_K a_K^m(I)\ \phi_K\ \mathcal{D}^I_{MK} \quad , \tag{16}$$

where the $a_K^m(I)$ are the calculated amplitudes, ϕ_K signifies a particular input configuration--0qp or 2qp in our cases--and the $\mathcal{D}^I_{MK}$ is the usual rotational wave function. The B(E2) value between two such states can be written:

$$B(E2;I+2,n \to I,m) = \sum_{\mu M'} |\langle IM',m|M(E2,\mu)|I+2\ M,n\rangle|^2 \tag{17}$$

where $M(E2,\mu)$ is the usual E2 operator. In evaluating eq. (17) it is clear that the B(E2) values between components ϕ_K and $\phi_{K'}$ are of single particle strength or smaller unless K = K', in which case they are the enhanced rotational values, $\frac{5}{16\pi} Q_0^2$. Keeping only the enhanced terms gives:

$$B(E2;I+2,n \to I,m) = \frac{5}{16\pi} Q_0^2 \left[\sum_K \langle I+2\ K\ 2\ 0|I+2\ 2\ I\ K\rangle a_K^m(I)\ a_K^n(I+2)\right]^2 \quad . \tag{18}$$

For large I the above Clebsch-Gordan coefficients are virtually independent of

K, and approach the limit, $\sqrt{3/8}$. Eq. (18) can then be written:

$$B(E2;\ I+2,n \rightarrow I,m\ ) \approx \frac{3\cdot 5}{8\cdot 16\pi}\ Q_0^2\ [\sum_K a_K^m(I)\ a_K^n(I+2)]^2 \quad . \tag{19}$$

The remaining summation in eq. (19) looks like the one occurring in an orthogonality integral, which would be written:

$$\sum_K a_K^m(I)\ a_K^{m'}(I) = \delta_{m,m'} \quad . \tag{20}$$

Since we have argued above that the states n look much like the states m for n = m, it follows from eqs. (19) and (20) that

$$B(E2;\ I+2,n \rightarrow I,m\ ) \approx \frac{15}{128\pi}\ Q_0^2\ \delta_{m,n} \quad , \tag{21}$$

that is, the transitions having solid lines in fig. 31 have the full rotational strength, and those with dashed lines vanish. It is easy to see that transitions of the type I+2,n → I+2,n' also vanish, since in this approximation the Clebsch-Gordan coefficient again factors out and the sum in eq. (19) now really <u>is</u> the orthogonality integral. These are precisely the selection rules needed in section 4.1 to bring the population down in spin very quickly, but keep it spread over several bands. The population then feeds rather sharply into the ground band at a critical spin value. The reason for this is that the ground band intersects the 2qp bands rather sharply near this spin value and the assumption that the matrices look nearly the same for adjacent spin values is then not valid, particularly relative to the ground band. Thus, at the point where the ground band intersects other bands, not only does the developing energy gap (with decreasing I) favor population of the ground band, but the B(E2) values for this population also peak in just this region. This seems to provide a

very general explanation for rapid population of the ground band near this point, in accordance with the observations.

To show that the present calculations can really fit the detailed rotational-band spacings, I have compared in fig. 32 a calculation with the data on ^{158}Dy taken by Tieberger et al.[27]). There is one parameter in the calculation. It was made at a time when we did not include the recoil term in the diagonalization, in which case the Coriolis effects turn out to be too strong. Thus for the calculation shown in fig. 32 all Coriolis matrix elements were reduced by a factor of 0.7, which was adjusted to give the kink at about the right place. Inclusion of the recoil term has very much the same effect, with no parameter involved. The agreement in fig. 32 seems excellent, and could be easily improved by varying slightly some of the other numbers going into the calculation. The slope on the experimental curve at very low spin values is probably a feature that does not come naturally out of such a model. It is, perhaps, the effect of the rotation on the moment of inertia--the so-called Coriolis anti-pairing effect. But at higher spin values, around the kink, the present calculations can account very well for the behavior.

It is easy to make predictions using this model, since the calculations are rather simple. Two expected trends will be discussed. First, the Coriolis effects are very sensitive to λ for reasons discussed in section 2. They are large for low λ values, and small for high λ values. Fig. 33 shows the results of diagonalizing the even-even case for various λ values, keeping everything else fixed. One sees fairly violent behavior (S-shapes) for low λ values, moderate behavior (kinks) for intermediate λ values, and quite smooth behavior for high λ values. There is some hint that this trend may occur in the

experimental data, but much more data on heavy Yb, Hf, and W nuclei are needed to test this. Another prediction we can make is that when $\hbar^2/2\mathfrak{I}$ becomes larger and λ is low the S-shapes can become quite large (see fig. 33), resulting in apparent moments of inertia that temporarily exceed the rigid body value. This kind of behavior seems unlikely on a pairing-collapse model. Thus data on still lighter Er and Dy nuclei might serve to distinguish between these models.

4.4. Summary

It seems that this model, which takes into account Coriolis effects in the 2qp states, can account very nicely for the experimental data existing in the light rare-earth even-even nuclei. This includes data on both the heavy-ion feeding and the detailed rotational spacings. The agreement seems so close that one can perhaps make an even stronger statement of the situation, as follows. If the events occurring around I = 16 in these even-even nuclei are not due to Coriolis effects, then one must assume that something has seriously weakened the Coriolis force; because all the simple calculations and expectations from the odd-A nuclei suggest that rather large Coriolis effects <u>should</u> be present. This statement is not quite so strong as it might sound, since there are some reductions of the Coriolis matrix elements in odd-A nuclei that are not yet really understood. If these reductions should become much larger in the even-even nuclei, then the effects I have described would only occur at higher spin values. However, at the present time it seems most likely to us that the observed features are these Coriolis effects.

5. Conclusion

We have traced the Coriolis effects in nuclei from the point where they are small perturbations in good rotational spectra, to the point where they apparently dominate the low-energy spectrum. The situation for a particular case depends on the relationship of the rotational energy to the energy coupling the particle to the non-spherical part of the potential. If the latter energy is much larger, good rotational spectra exist, whereas if it vanishes the system is spherically symmetric with no energy splitting of the multiplets formed by coupling a particle to a core state. With the assumptions and simplifications made in sections 2 and 3, it is easy to make calculations anywhere between these limits. Adjacent to each limit, one finds regions where a perturbation treatment could apply. This would be a particle-core weak coupling model near the spherical limit, and a Coriolis perturbation approach near the good rotational region. If the Fermi surface is near high-Ω levels, then the two perturbation regions merge into each other, and one changes rather quickly from a spherical region into one of reasonably good rotors. But if the Fermi surface is near low-Ω states then the Coriolis effects are large, and there is a broad region where neither of these schemes is very good. In this region another coupling scheme applies where the particle angular momentum has sharp values along the rotational axis (or x-axis). In this case the lowest-lying states of a given spin have the particle angular momentum parallel to this axis, resulting in the so-called decoupled levels. These levels are easily recognized by the fact that their energy spacings are just equal to those of the even-even core, and it appears that levels with this property occur rather commonly in heavy odd-A nuclei. It may also be that such configurations are

involved in the yrast states in even-even nuclei at very high spin values. Much remains to be learned about this kind of calculation and how it applies to nuclei, but at present this approach looks quite promising.

Acknowledgment

I am indebted to Dr. R. M. Diamond for continuing discussions on the subjects discussed here, and for his comments on this manuscript. Many other people have also made helpful suggestions and comments related to the various aspects of this problem.

References

1. A. Bohr, Dan. Mat. Fys. Medd. 26, no. 14 (1952)
2. A. K. Kerman, Dan. Mat. Fys. Medd. 30, no. 15 (1956)
3. S. G. Nilsson, Dan. Mat. Fys. Medd. 29, no. 16 (1955)
4. D. J. Rowe, Nucl. Phys. 61, 1 (1965)
5. R. T. Brockmeier, S. Wahlborn, E. J. Seppi, and F. Boehm, Nucl. Phys. 63, 102 (1965)
6. A. Bohr and B. R. Mottelson, Nuclear Structure, Benjamin, New York, New York, Vol. 1 (1969), Vols. 2 and 3, to be published.
7. F. S. Stephens, M. D.Holtz, R. M. Diamond, and J. O. Newton, Nucl. Phys. A115, 129 (1968)
8. S. A. Hjorth, H. Ryde, K. A. Hagemann, G. Løvhøiden, and J. C. Waddington, Nucl. Phys. A144, 513 (1970)
9. L. Grodzins, Phys. Letters 2, 88 (1962)
10. P. Vogel, Phys. Letters 33B, 400 (1970)
11. A. de-Shalit, Phys. Rev. 122, 1530 (1961)
12. B. R. Mottelson, private communication, June 1972
13. J. R. Leigh, K. Nakai, K.H. Maier, F. Pühlhofer, R. M. Diamond, and F. S. Stephens, to be published.
14. K. Nakai and P. Kleinheinz, to be published
15. F. S. Stephens, R. M. Diamond, J. R. Leigh, T. Kammuri, and K. Nakai, Phys. Rev. Letters, in press.
16. J. O. Newton, S.D. Cirilov, F. S. Stephens, and R. M. Diamond, Nucl. Phys. A148, 593 (1970).

17. J. R. Leigh, J. O. Newton, L. A. Ellis, M. C. Evans, and M. J. Emmott, Nucl. Phys. A183, 177 (1972)

18. J. Frana, A. Spalek, M. Fiser, and A. Kokes, Nucl. Phys. A165, 625 (1972)

19. D. Benson, M. Maier, R. M. Diamond, and F. S. Stephens, to be published

20. F. B. Malik and W. Sholz, Phys. Rev. 150, 919 (1966); 153, 1071 (1967); and others

21. J. O. Newton, F. S. Stephens, R. M. Diamond, W. H. Kelley, and D. Ward, Nucl. Phys. A141, 361 (1970)

22. J. R. Grover, Phys. Rev. 157, 832 (1967); J. R. Grover and J. Gilat, Phys. Rev. 157, 862 (1967); ibid 814; ibid 823

23. B. R. Mottelson, The Nuclear Structure Symposium of the Thousand Lakes, Joutsa, Finland, August 1970; Fifth Nordic-Dutch Accelerator Symposium, Ebeltoft, Denmark, May 1971

24. A. Johnson, H. Ryde, and J. Sztarkier, Phys. Letters 34B, 605 (1971)

25. B. R. Mottelson and J.G. Valatin, Phys. Rev. Letters 5, 511 (1960)

26. F. S. Stephens and R.S. Simon A183, 257 (1972)

27. P. Thieberger, A.W. Sunyar, P. C. Rogers, N. Lark, O. C. Kistner, E. der Matoesian, S. Cockavi, and E. H. Auerbach, Phys. Rev. Letters 28, 972 (1972)

Figure Captions

Fig. 1. The ^{183}W rotational bands as treated by Kerman.

Fig. 2. The solid lines are the Nilsson solutions for the $h_{11/2}$ orbital ($\mu = 0.70$) as a function of deformation. The dashed lines are the energies given by eq. (12). The vertical line marks $\beta = +0.275$, and its intersections with the Nilsson lines represent the energies of the various component levels at that deformation.

Fig. 3. The $j_{15/2}$ bands in ^{235}U (as calculated from eqs. (6) and (9)) prior to the Coriolis diagonalization. The matrix elements of the operator $j_{\pm}$ as calculated from the Nilsson wave functions are also shown. Only a few rotational levels of each band are indicated.

Fig. 4. Levels Coulomb excited in ^{235}U.

Fig. 5. Rotational spacings of bands in ^{235}U. The points are the experimental data, with the height of a point covering the error limits, and the lines correspond to the spacings obtained from the one-parameter Coriolis calculation.

Fig. 6. This plot is like fig. 5, except (1) the lines correspond to the three-parameter Coriolis calculation, and (2) the ordinate scale has been doubled.

Fig. 7. The experimental and calculated positive-parity levels in $^{161,163,165}Er$ according to ref. [8].

Fig. 8. Rotational spacings of the positive-parity band in the three Er nuclei. Some other bands are plotted on this figure but are not relevant to the present discussion.

Fig. 9. The results of diagonalizing eq. (4) for various β values are given for the lowest state of each spin up to I = 23/2 (the second I = 11/2 state is included). The ordinate is the eigenvalue less the lowest I = 11/2 eigenvalue, in units of E_{2+}, and the abcissa is β. The Fermi surface, λ, is below the entire orbital for this calculation.

Fig. 10. The Coriolis effects on a spinning wheel constrained to turn with a turntable (a) tend to produce the configuration shown in (b). For the argument made in the text, the axis of the wheel in (b) should also be fastened to the turntable.

Fig. 11. The three coupling schemes are indicated. At the top is the strong-coupling scheme, with sharp projections on the z axis. At the bottom there are two schemes, one with sharp values of R, and the other with sharp projections of j on the rotational (vertical) axis.

Fig. 12. A comparison of ground-band levels in some Ba isotopes with the negative-parity bands in the neighboring La nuclei. In most cases (energy zero in parentheses) the La 11/2-level is not the ground state, and its energy has been subtracted from all levels shown for that isotope.

Fig. 13. Like fig. 9, except that the abcissa is β (top) or the cube root of the total splitting of the $h_{11/2}$ orbital in units of E_{2+} (bottom). The Fermi surface, λ, is always located on the Ω = 1/2 state, so that in the limit of very large β, the levels will become a pure Ω = 1/2 band with a decoupling parameter of -6. The dots show the effect of diagonalizing eq. (14) instead of eq. (4), where B and C were adjusted to fit the lowest few levels in ^{126}Ba (see section 3.4.).

Fig. 14. The effect of varying λ is shown for a fixed value of β = 0.25. At the top, the location of the $h_{11/2}$ component levels is shown.

Fig. 15. A portion of the Nilsson diagram for protons in the region of Au. The main interest here is in the $h_{9/2}$ and $h_{11/2}$ orbitals, which are fully drawn. The ground states of Au and Tl are in the $s_{1/2}$ and $d_{3/2}$ orbitals which are partially drawn.

Fig. 16. Solution of eq. (4) for the $h_{9/2}$ orbital. Only the experimentally observed levels were drawn. The dots correspond to the experimental data from ^{199}Tl and ^{179}Re. The dashed lines correspond to solutions of eq. (14).

Fig. 17. A comparison of the experimental negative-parity levels in ^{199}Tl with those calculated according to eq. (4) and eq. (14). The dashed levels are tentative and should probably not be considered very seriously.

Fig. 18. Solutions of eq. (4) for the $h_{11/2}$ orbital with λ adjusted for Au (top) and Re (bottom). The dots show the experimental data for ^{195}Au and ^{179}Re.

Fig. 19. A comparison of the experimental negative-parity levels in ^{195}Au with those calculated according to eq. (4) and eq. (14).

Fig. 20. Excitation energy is plotted against angular momentum in a nucleus (with mass around 160) that is the product of an (^{40}Ar,4n) reaction. The populated energy and angular momentum range is shown, together with the proposed cascade pathway to the ground state.

Fig. 21. The reciprocal of $\hbar^2/2\mathcal{J}$ (defined from the transition energies) is plotted against the square of the rotational frequency for several light rare-earth nuclei. The value of $\hbar\omega$ is, to a good approximation, just the transition energy divided by two.

Fig. 22. The solid lines show the energies of two rotational bands as a function of I. The bands have different moments of inertia ($\hbar^2/2\mathcal{J}_1$ = 15 keV,

$\hbar^2/2\mathfrak{J}_2$ = 10 keV) and are arranged to intersect at I = 16. The dotted and dashed lines show the energies of the mixed bands resulting from cases B and C, respectively, in fig. 23.

Fig. 23. The ratio $\mathfrak{J}/\mathfrak{J}_2$ is plotted vs. ω^2 for the two bands in fig. 22. The horizontal lines connected by a dashed line correspond to no mixing between the bands, C corresponds to inter-band matrix elements comparable to the maximum gsb-2qp ones used in our calculations, B to matrix elements 3 times smaller, and A to ones 10 times smaller. We have used $\mathfrak{J} \approx \frac{(4I-2)}{(E_I-E_{I-2})}$ and $\hbar\omega \approx \frac{2(I-1)(E_I-E_{I-2})}{(4I-2)}$, which differ slightly from those others have used, but not significantly.

Fig. 24. Rotational-level spacings to be expected from an $i_{13/2}$ particle in (left) a normal rotational band and (right) a decoupled band.

Fig. 25. The I = 17/2 to I = 13/2 energy difference in units of E_{2+} is plotted against neutron number in the light Er region. The coupled and decoupled limits for this quantity are shown.

Fig. 26. Simple estimates are shown of the ground-band energy in an even-even nucleus (solid line), the energy of the decoupled state based on two $i_{13/2}$ particles (dashed line), and the energy of a state with no pairing correlations (dotted line).

Fig. 27. The coupling scheme discussed in the text. It should not be inferred from this sketch that all these quantities have sharp values simultaneously.

Fig. 28. Placement of particles in the states based on the $i_{13/2}$ orbital in an even-even nucleus with a Fermi surface, λ. The left side of the figure represents the most probable situation for the ground state, whereas the right side shows a low-lying 2-quasiparticle state. Many levels from other orbitals would be intermixed with these, but for simplicity are not shown.

Fig. 29. The ten states possible considering only 2qp states in the Ω = 1/2, 3/2, and 5/2 components of the $i_{13/2}$ orbital plus the ground state (0qp). The interconnecting lines show the locations of non-zero Coriolis matrix elements.

Fig. 30. The lowest two solutions of the even-even case for β = 0.3 (solid lines), β = 0.2 (dashed lines), and β=0.1 (dotted lines). The numbers represent the total population passing through each level.

Fig. 31. A schematic illustration of the lowest three solutions for spins I and I+2, with some of the interconnecting E2 transitions indicated.

Fig. 32. A comparison of the calculated and observed values of $2\mathcal{J}/\hbar^2$ vs. rotational frequency for ^{158}Dy.

Fig. 33. The variation of the calculated rotational properties with the Fermi surface, λ, is shown.

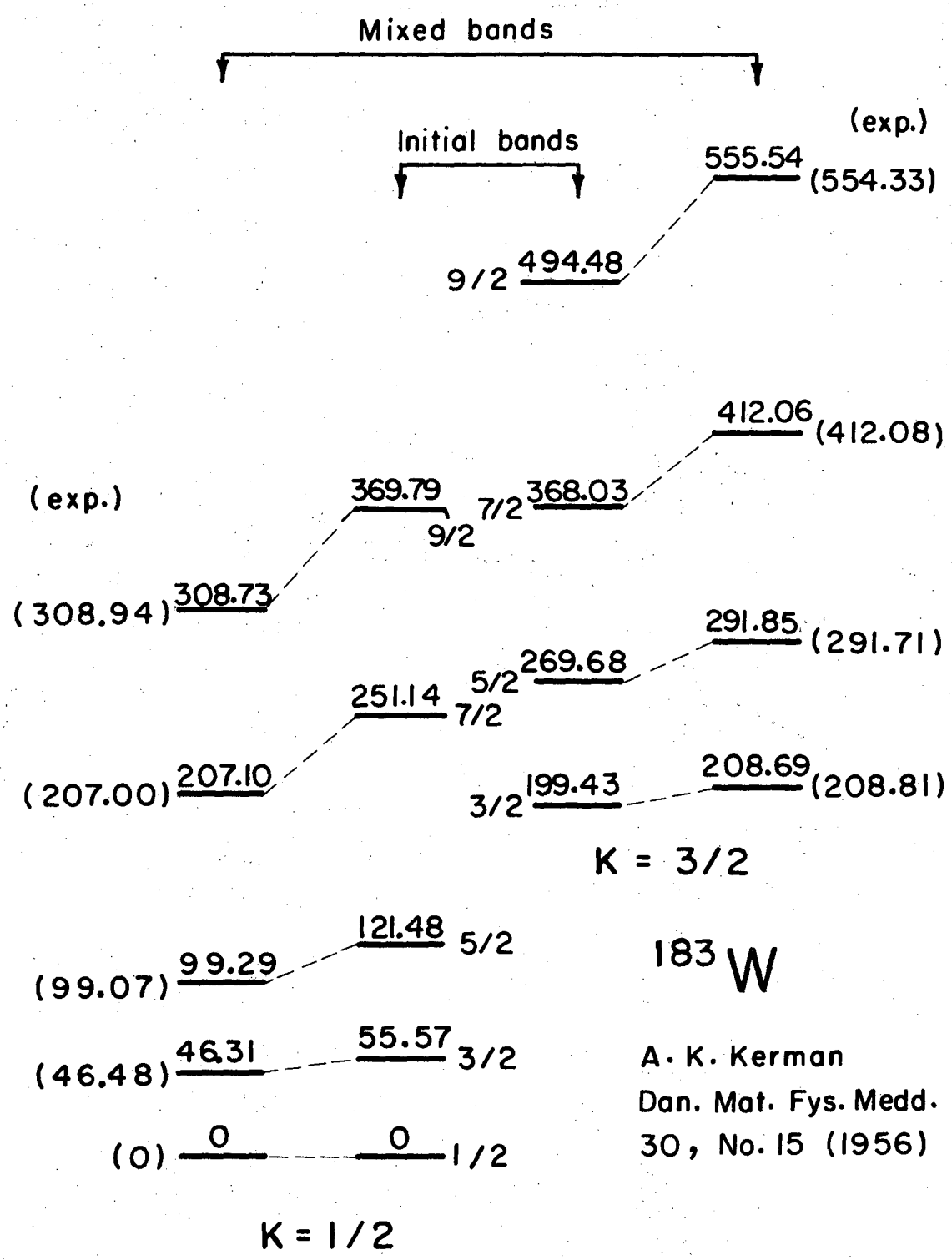
Mixed bands
Initial bands
(exp.)
555.54
(554.33)
494.48
9/2
412.06
(412.08)
(exp.)
369.79
9/2
7/2
368.03
(308.94)
308.73
291.85
(291.71)
269.68
5/2
251.14
7/2
(207.00)
207.10
208.69
(208.81)
3/2
199.43
K = 3/2
121.48
5/2
(99.07)
99.29
(46.48)
46.31
55.57
3/2
(0)
0
0
1/2
K = 1/2
183 W
A. K. Kerman
Dan. Mat. Fys. Medd.
30, No. 15 (1956)
XBL728-3693

Fig. 1

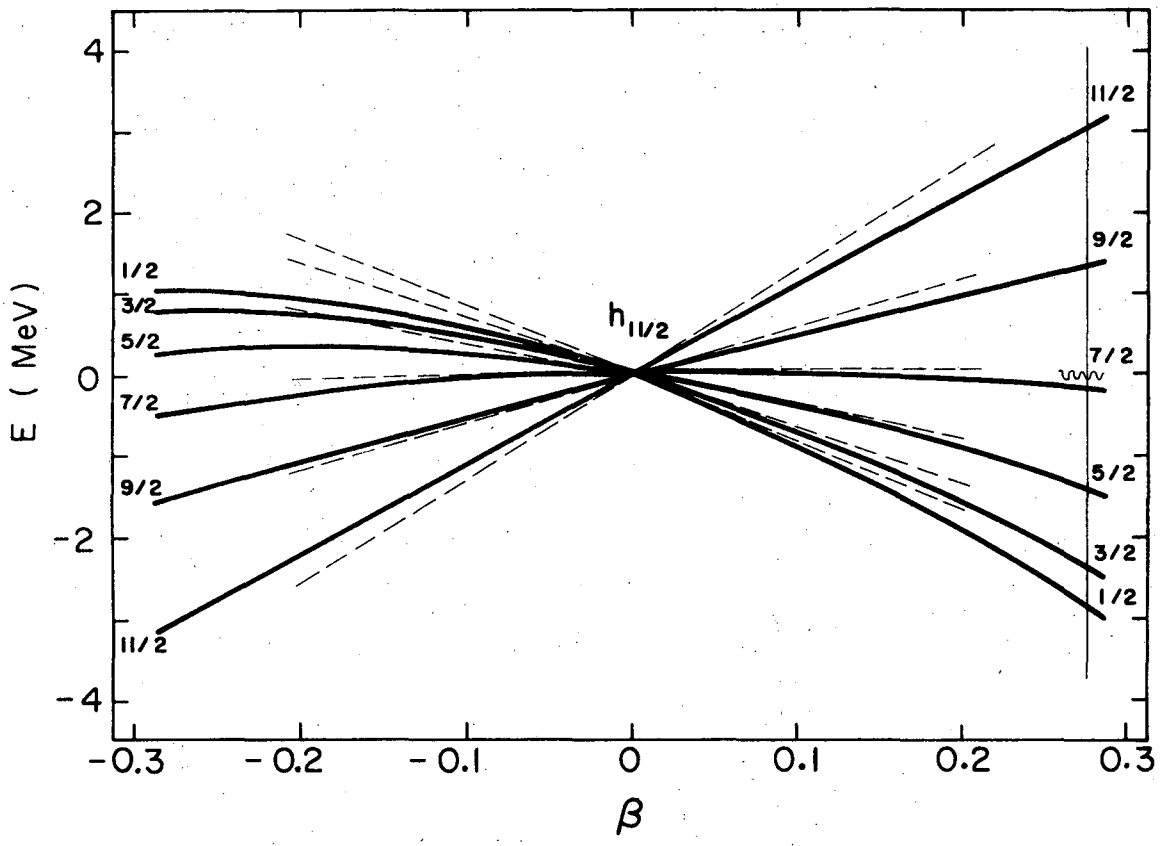
4
2
0
-2
-4
E (MeV)
-0.3
-0.2
-0.1
0
0.1
0.2
0.3
β
h11/2
1/2
3/2
5/2
7/2
9/2
11/2
11/2
9/2
7/2
5/2
3/2
1/2
XBL728-3692

Fig. 2

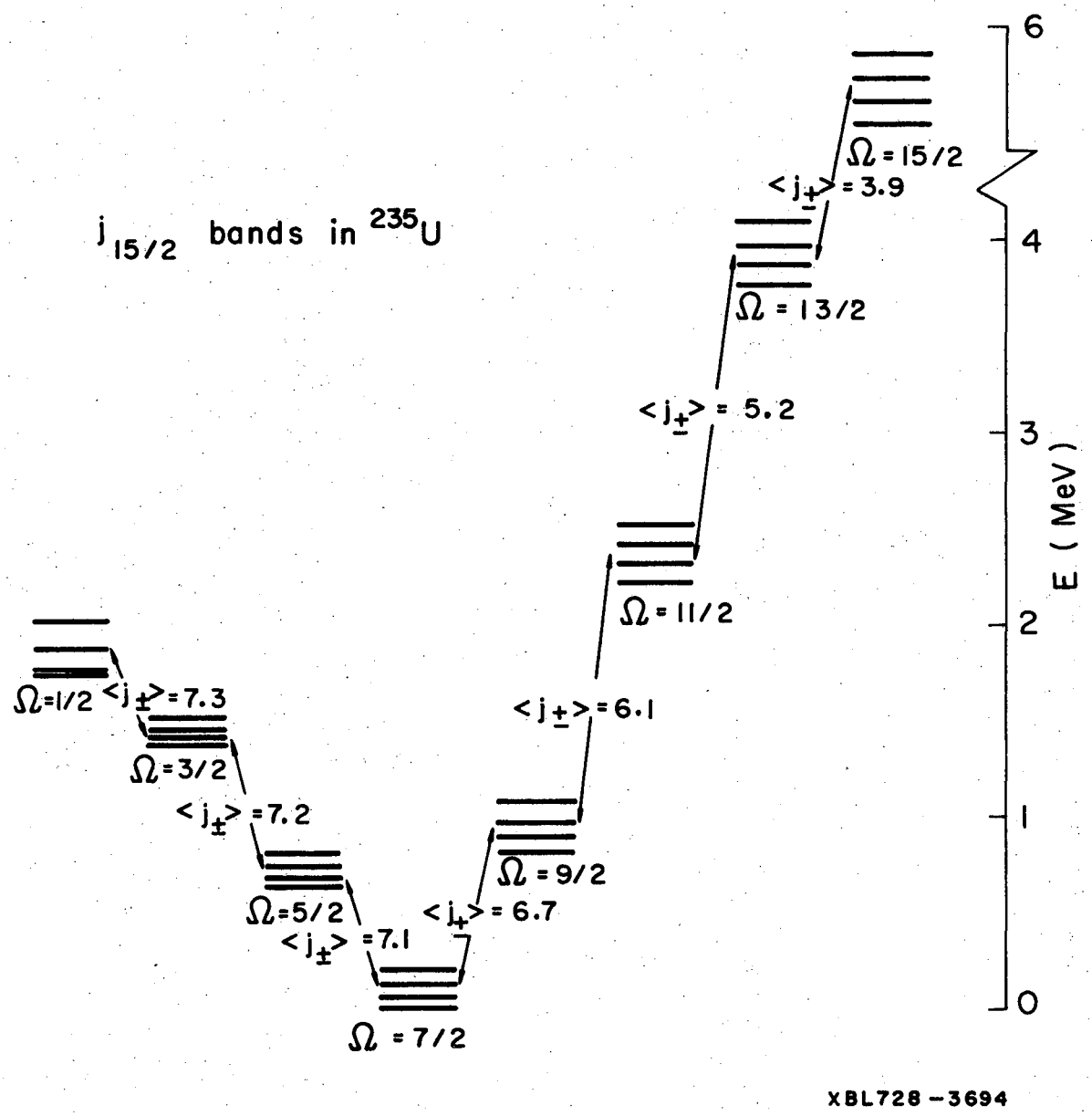
$j_{15/2}$ bands in ^{235}U
Ω=1/2
<j±>=7.3
Ω=3/2
<j±>=7.2
Ω=5/2
<j±>=7.1
Ω=7/2
<j+>=6.7
Ω=9/2
<j±>=6.1
Ω=11/2
<j±>=5.2
Ω=13/2
<j±>=3.9
Ω=15/2
E (MeV)
0
1
2
3
4
6
XBL728-3694

Fig. 3

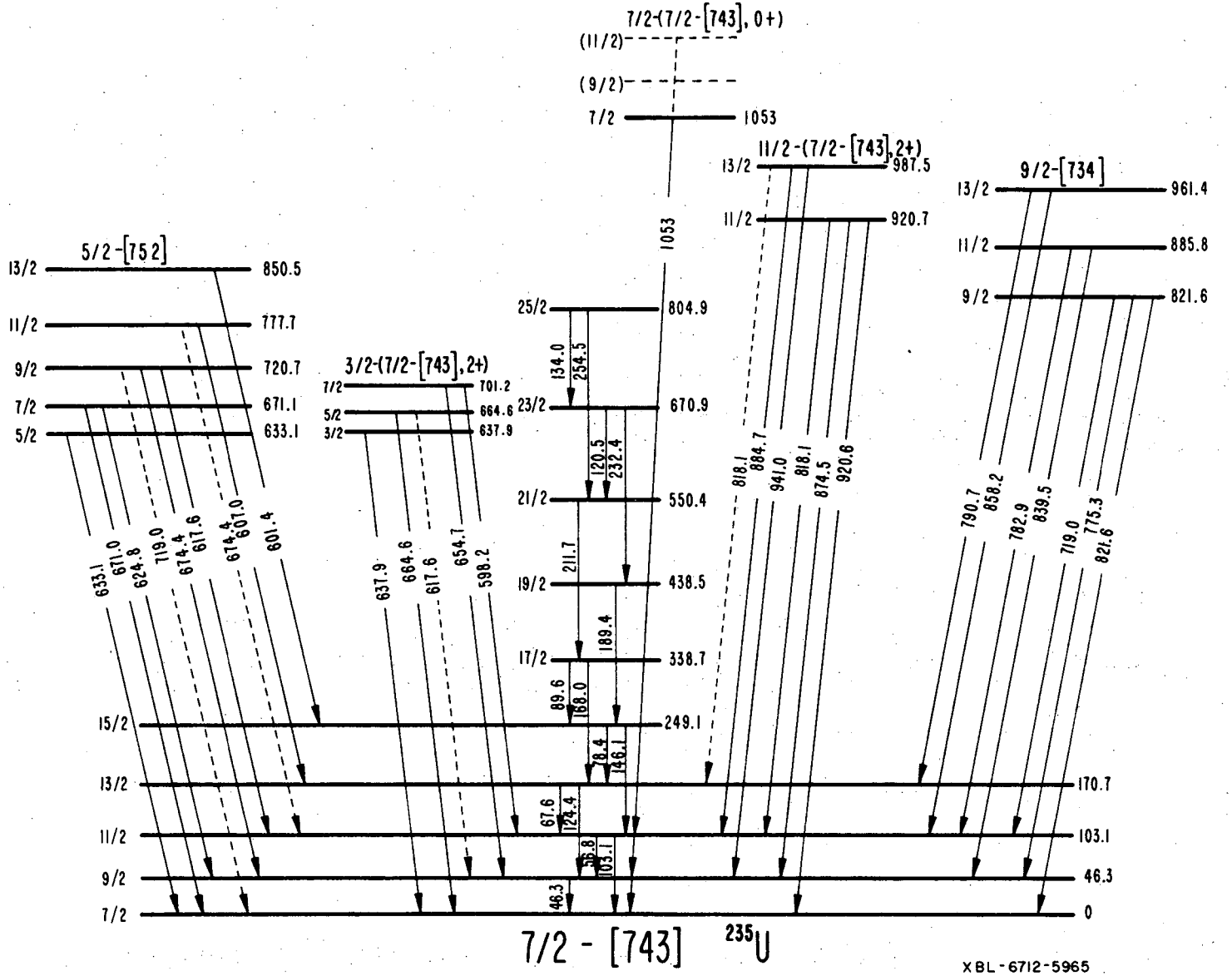
7/2-(7/2-[743], 0+)
(11/2)
(9/2)
7/2 1053
11/2-(7/2-[743],2+)
13/2 987.5
11/2 920.7
9/2-[734]
13/2 961.4
11/2 885.8
9/2 821.6
5/2-[752]
13/2 850.5
11/2 777.7
9/2 720.7
7/2 671.1
5/2 633.1
3/2-(7/2-[743],2+)
7/2 701.2
5/2 664.6
3/2 637.9
1053
25/2 804.9
23/2 670.9
21/2 550.4
19/2 438.5
17/2 338.7
15/2 249.1
13/2 170.7
11/2 103.1
9/2 46.3
7/2 0
134.0
254.5
120.5
232.4
211.7
189.4
89.6
188.0
78.4
146.1
67.6
124.4
56.8
103.1
46.3
633.1
671.0
624.8
719.0
674.4
617.6
674.4
601.0
601.4
631.9
664.6
617.6
654.1
598.2
818.1
884.7
941.0
818.1
874.5
920.8
790.7
858.2
782.9
839.5
719.0
775.3
821.6
7/2 - [743] 235U
XBL-6712-5965

Fig. 4

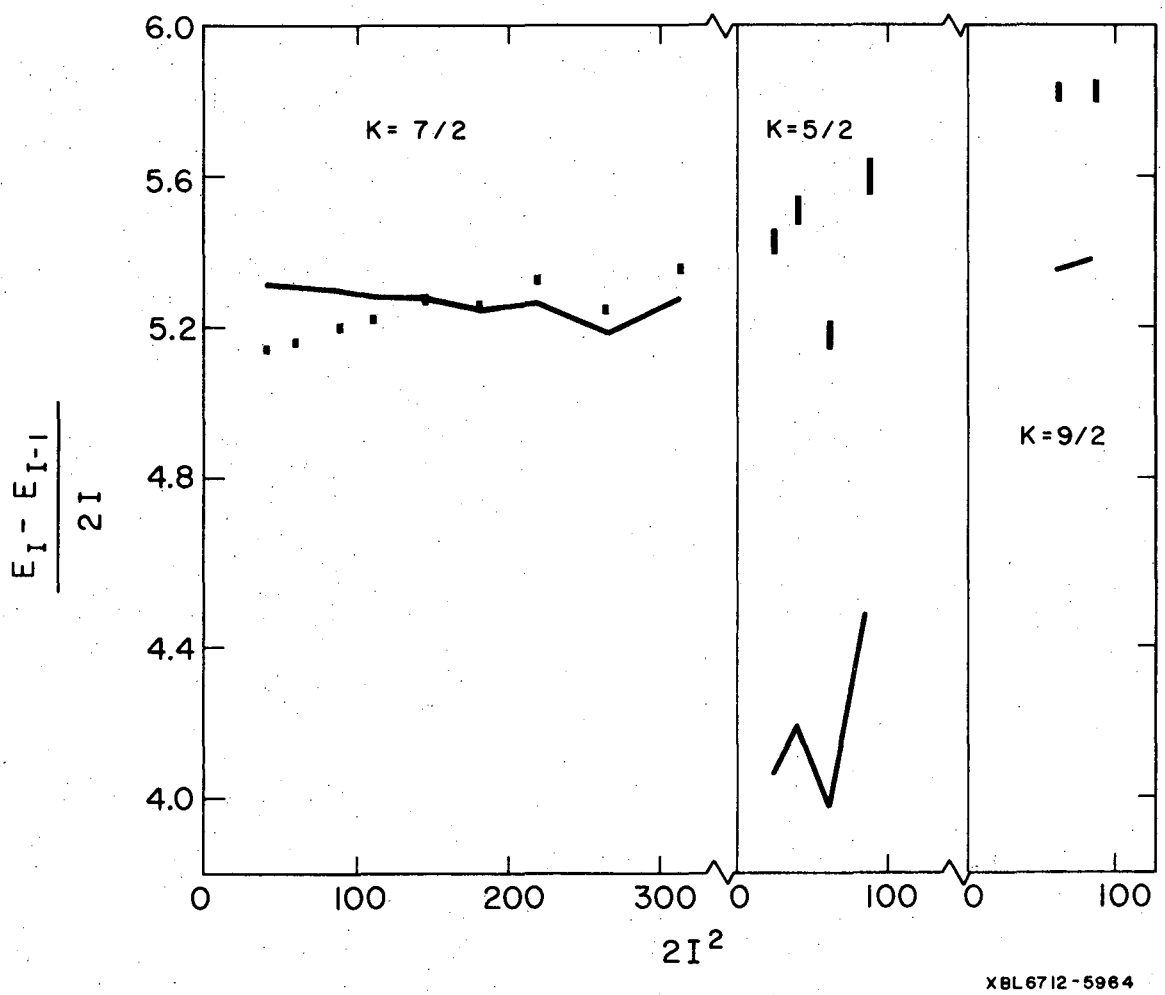
6.0
5.6
5.2
4.8
4.4
4.0
K= 7/2
K=5/2
K=9/2
0
100
200
300
0
100
0
100
$\frac{E_I - E_{I-1}}{2I}$
$2I^2$
XBL6712-5964

Fig. 5

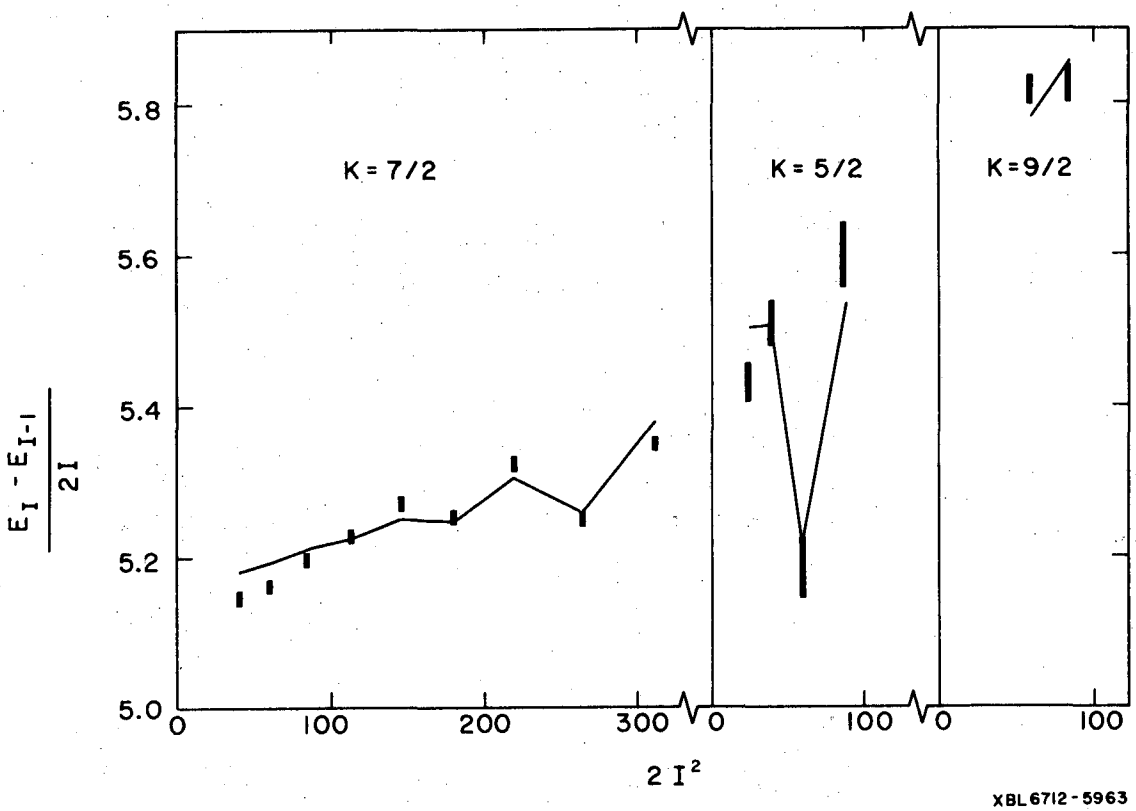
5.8
5.6
5.4
5.2
5.0
$\frac{E_I - E_{I-1}}{2I}$
K = 7/2
K = 5/2
K = 9/2
0
100
200
300
0
100
0
100
$2I^2$
XBL6712-5963

Fig. 6

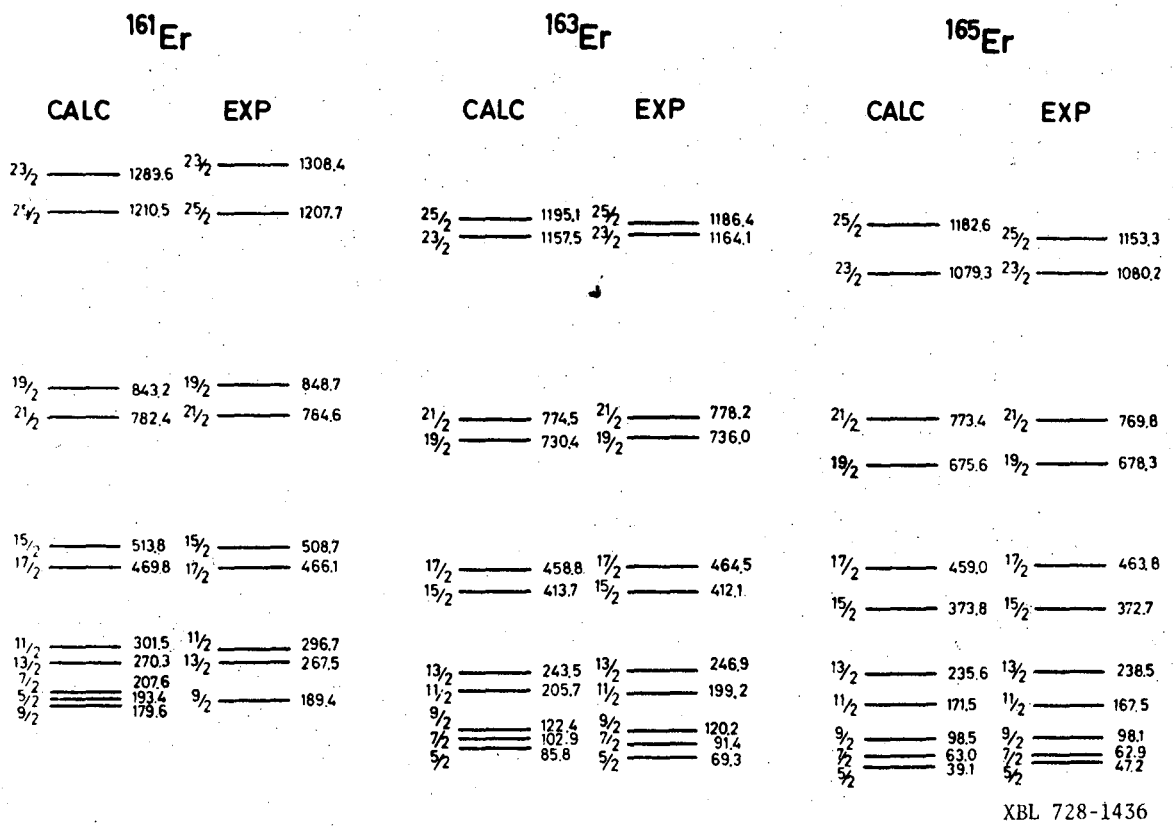

XBL 728-1436

Fig. 7

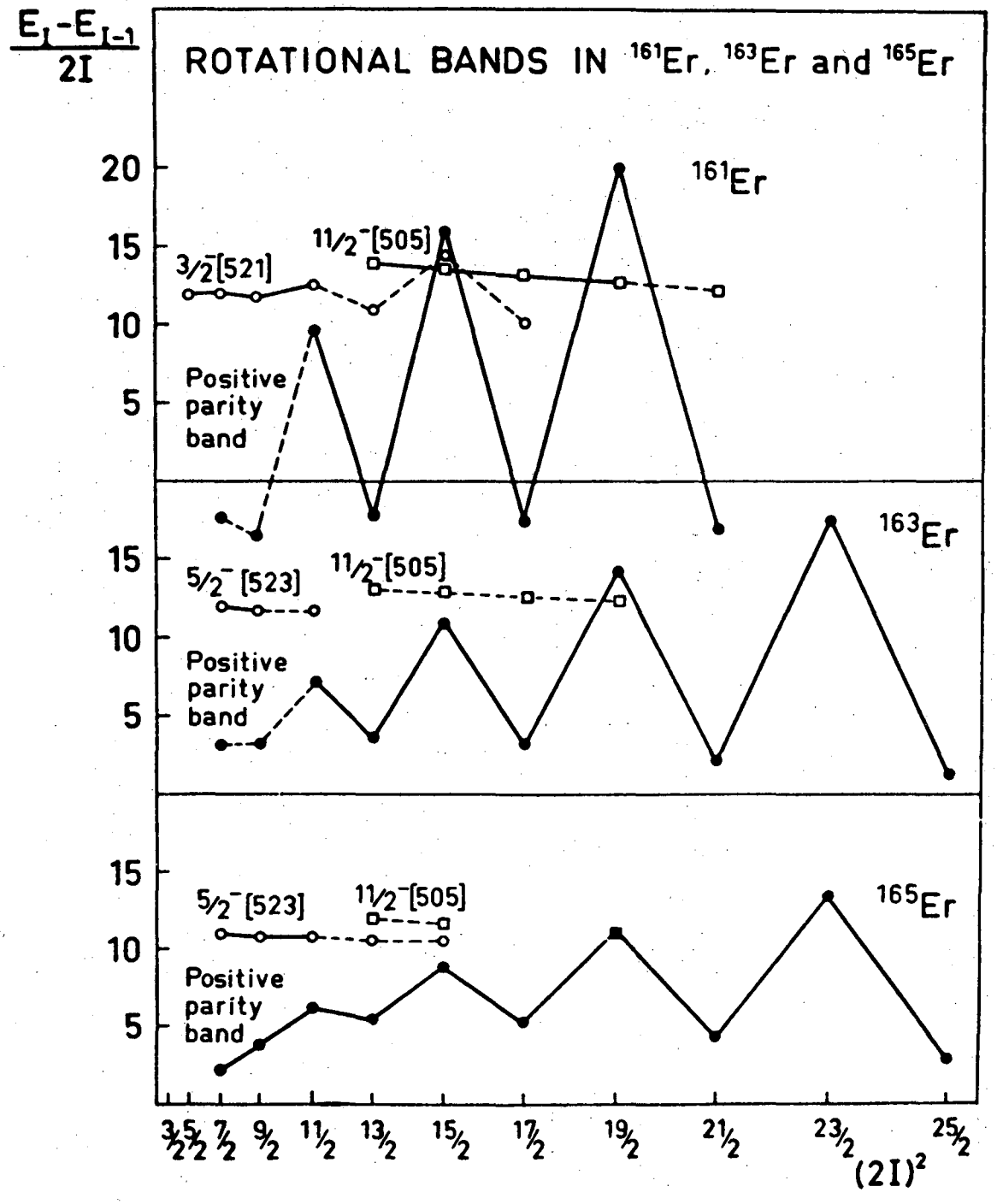
$\frac{E_I - E_{I-1}}{2I}$
ROTATIONAL BANDS IN ^{161}Er, ^{163}Er and ^{165}Er
^{161}Er
^{163}Er
^{165}Er
$3/2^-[521]$
$11/2^-[505]$
$5/2^-[523]$
Positive parity band
20
15
10
5
3/2 5/2 7/2 9/2 11/2 13/2 15/2 17/2 19/2 21/2 23/2 25/2
$(2I)^2$
XBL 728-1437

Fig. 8

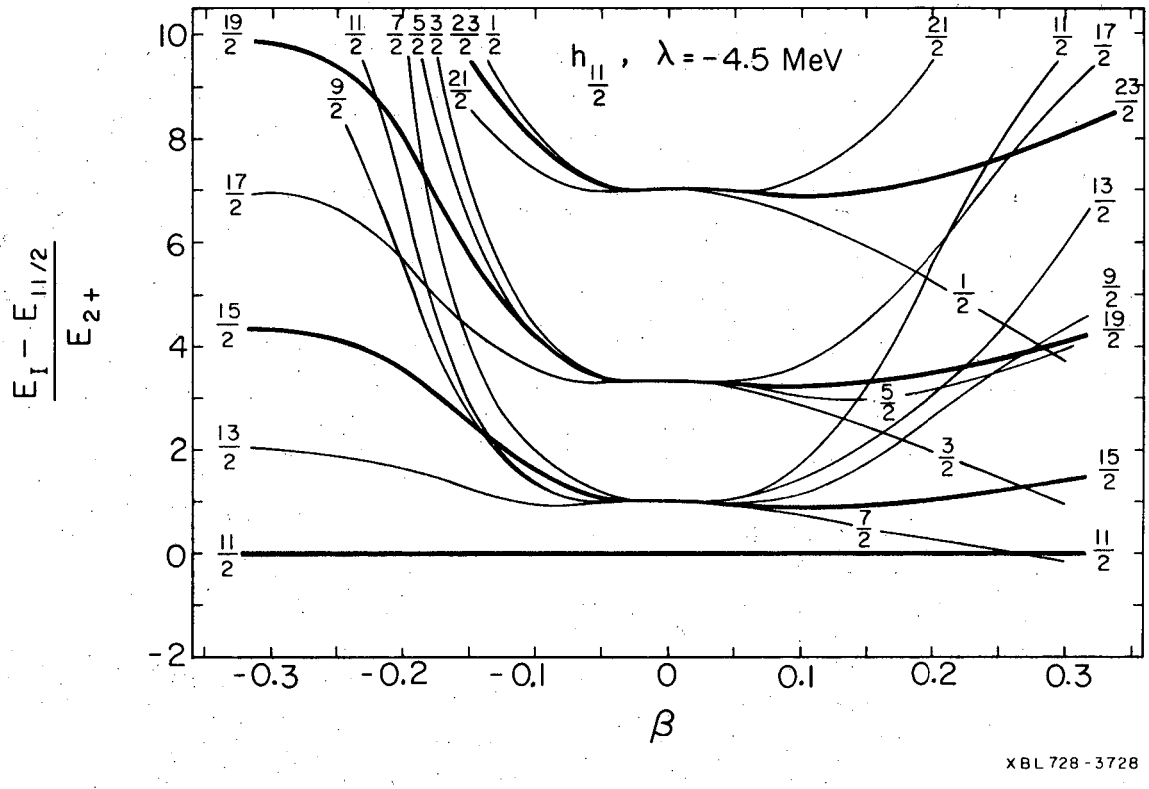

Fig. 9

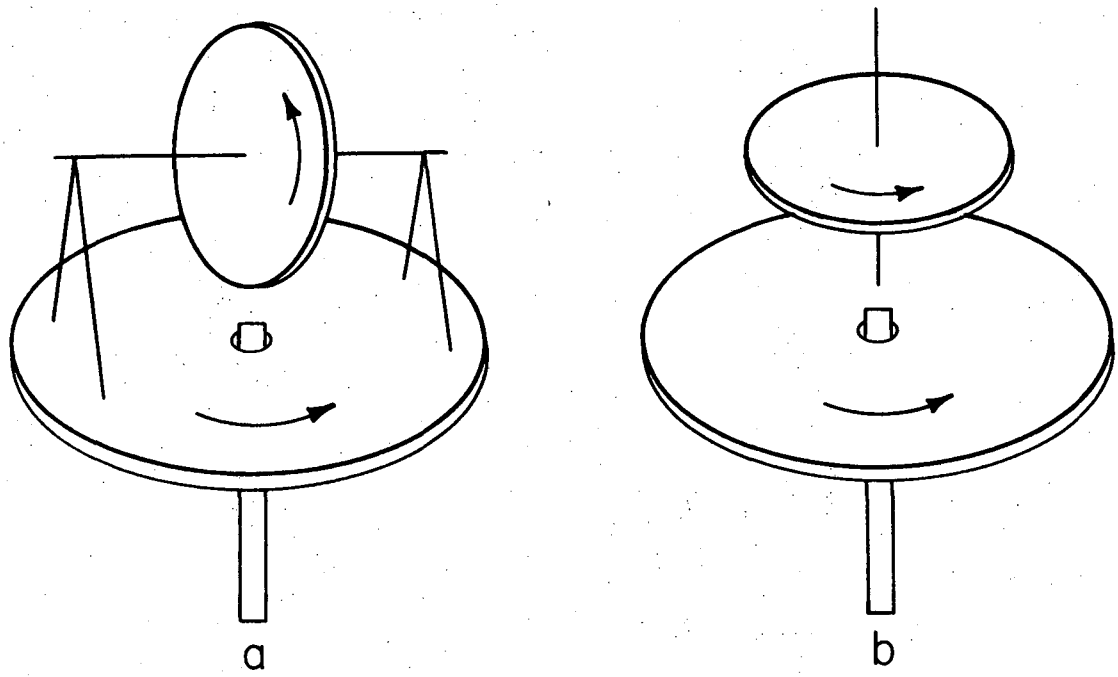

XBL7110 -4458

Fig. 10

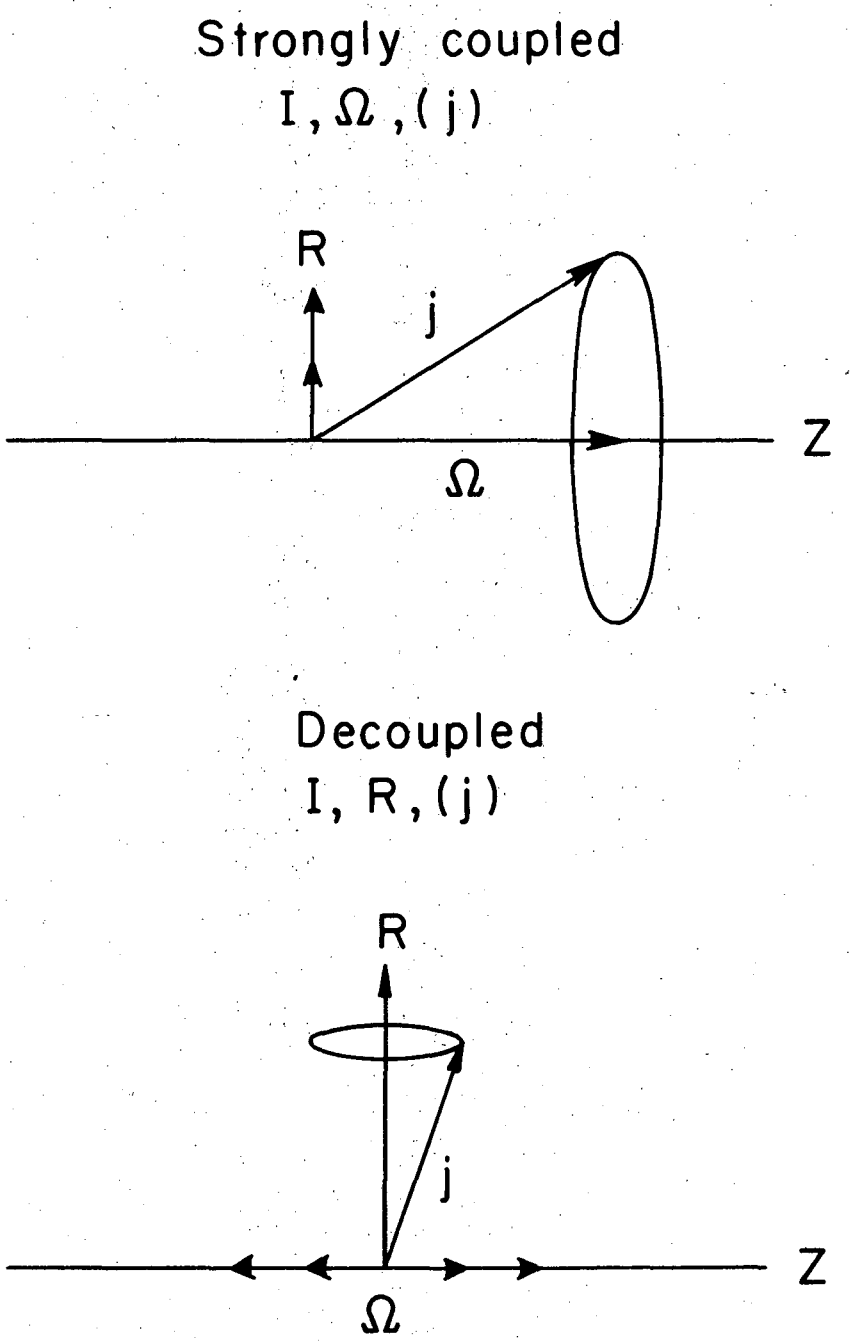

Fig. 11

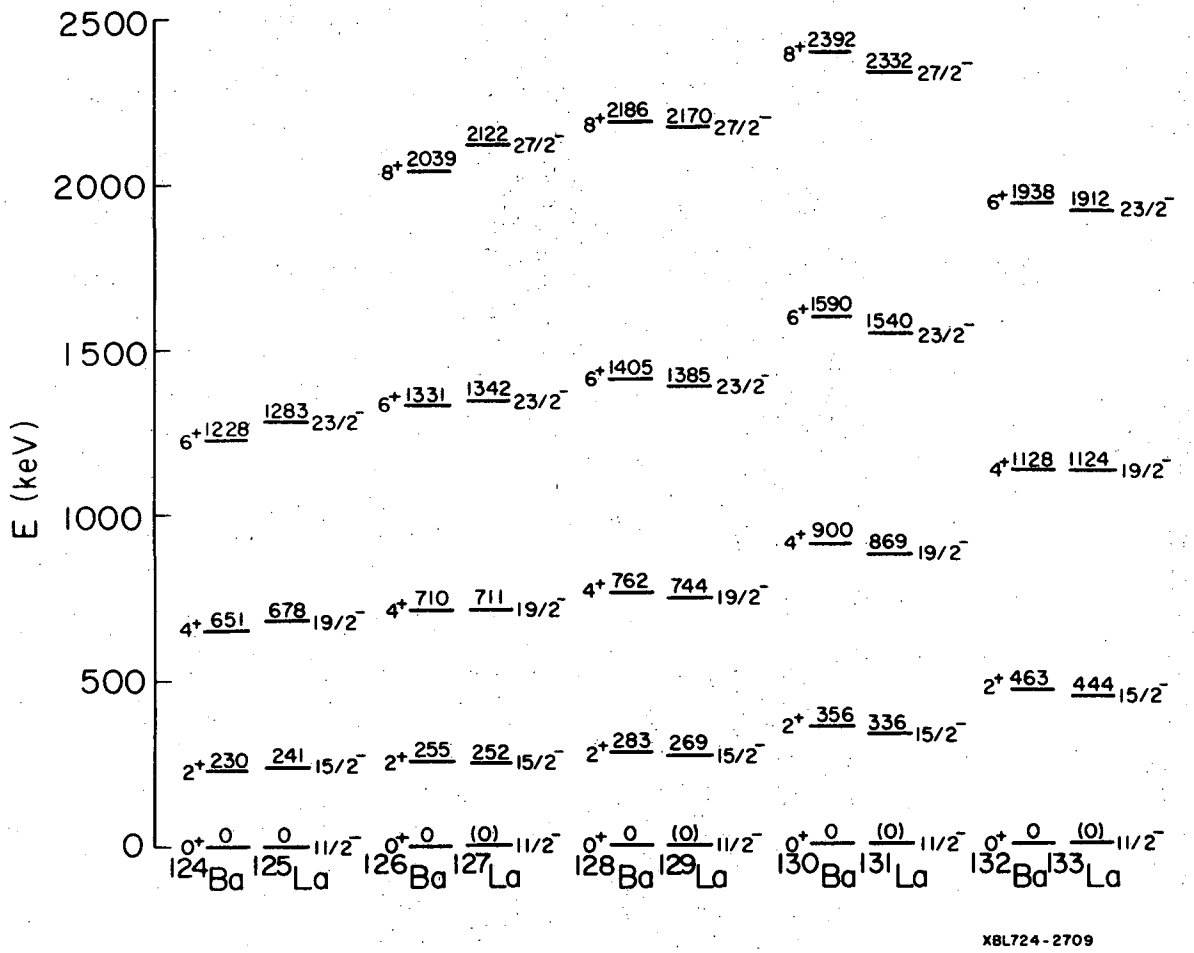
E (keV)
2500
2000
1500
1000
500
0
0+ 0
0 11/2-
2+ 230
241 15/2-
4+ 651
678 19/2-
6+ 1228
1283 23/2-
8+ 2039
2122 27/2-
2+ 255
252 15/2-
4+ 710
711 19/2-
6+ 1331
1342 23/2-
(0) 11/2-
8+ 2186
2170 27/2-
2+ 283
269 15/2-
4+ 762
744 19/2-
6+ 1405
1385 23/2-
8+ 2392
2332 27/2-
2+ 356
336 15/2-
4+ 900
869 19/2-
6+ 1590
1540 23/2-
2+ 463
444 15/2-
4+ 1128
1124 19/2-
6+ 1938
1912 23/2-
124Ba 125La 126Ba 127La 128Ba 129La 130Ba 131La 132Ba 133La
XBL724-2709

Fig. 12

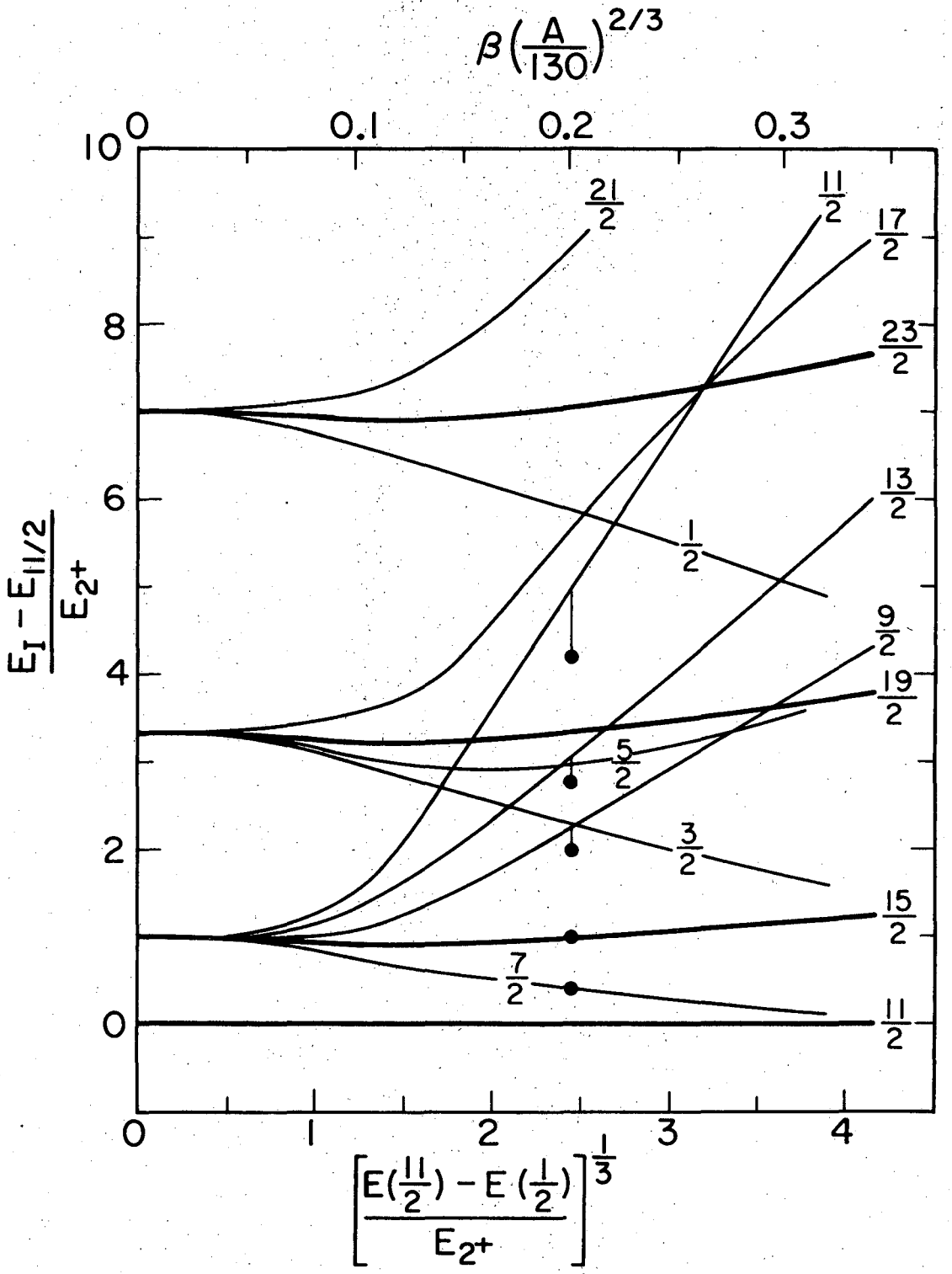
$\beta\left(\frac{A}{130}\right)^{2/3}$
0
0.1
0.2
0.3
10
8
6
4
2
0
$\frac{E_I - E_{11/2}}{E_{2^+}}$
21/2
11/2
17/2
23/2
13/2
1/2
9/2
19/2
5/2
3/2
15/2
7/2
11/2
0
1
2
3
4
$\left[\frac{E(\frac{11}{2}) - E(\frac{1}{2})}{E_{2^+}}\right]^{\frac{1}{3}}$
XBL724-2708

Fig. 13

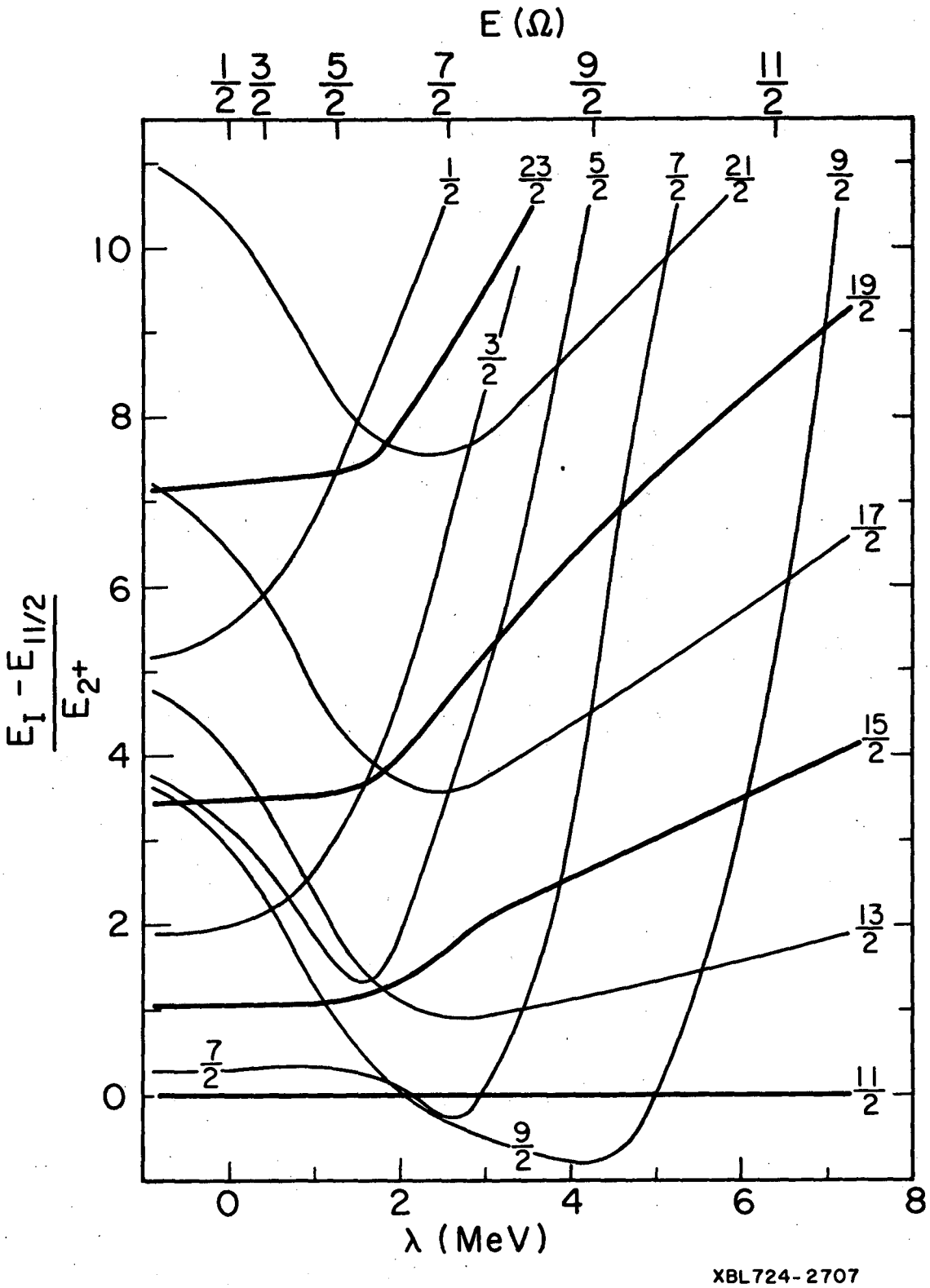
E (Ω)
1/2 3/2 5/2 7/2 9/2 11/2
1/2
23/2
5/2
7/2
21/2
9/2
19/2
3/2
17/2
15/2
13/2
7/2
11/2
9/2
$\frac{E_I - E_{11/2}}{E_{2^+}}$
0 2 4 6 8 10
0 2 4 6 8
λ (MeV)
XBL724-2707

Fig. 14

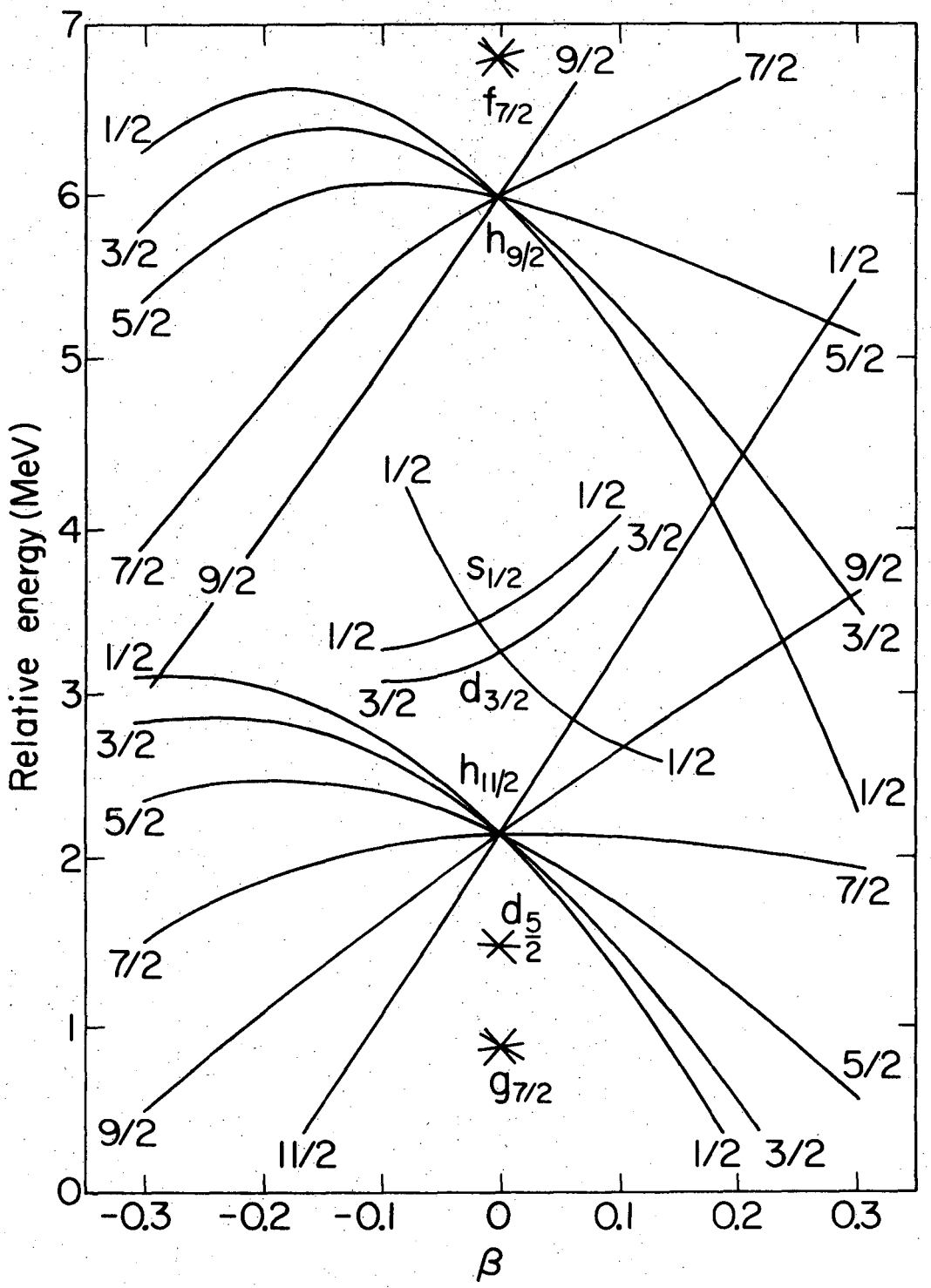
Relative energy (MeV)
β
9/2
f7/2
7/2
1/2
3/2
5/2
h9/2
1/2
5/2
1/2
1/2
3/2
s1/2
7/2
9/2
9/2
3/2
1/2
1/2
3/2
d3/2
3/2
h11/2
1/2
5/2
1/2
7/2
d5/2
7/2
5/2
g7/2
9/2
11/2
1/2
3/2
-0.3
-0.2
-0.1
0
0.1
0.2
0.3
0
1
2
3
4
5
6
7
XBL725-2887

Fig. 15

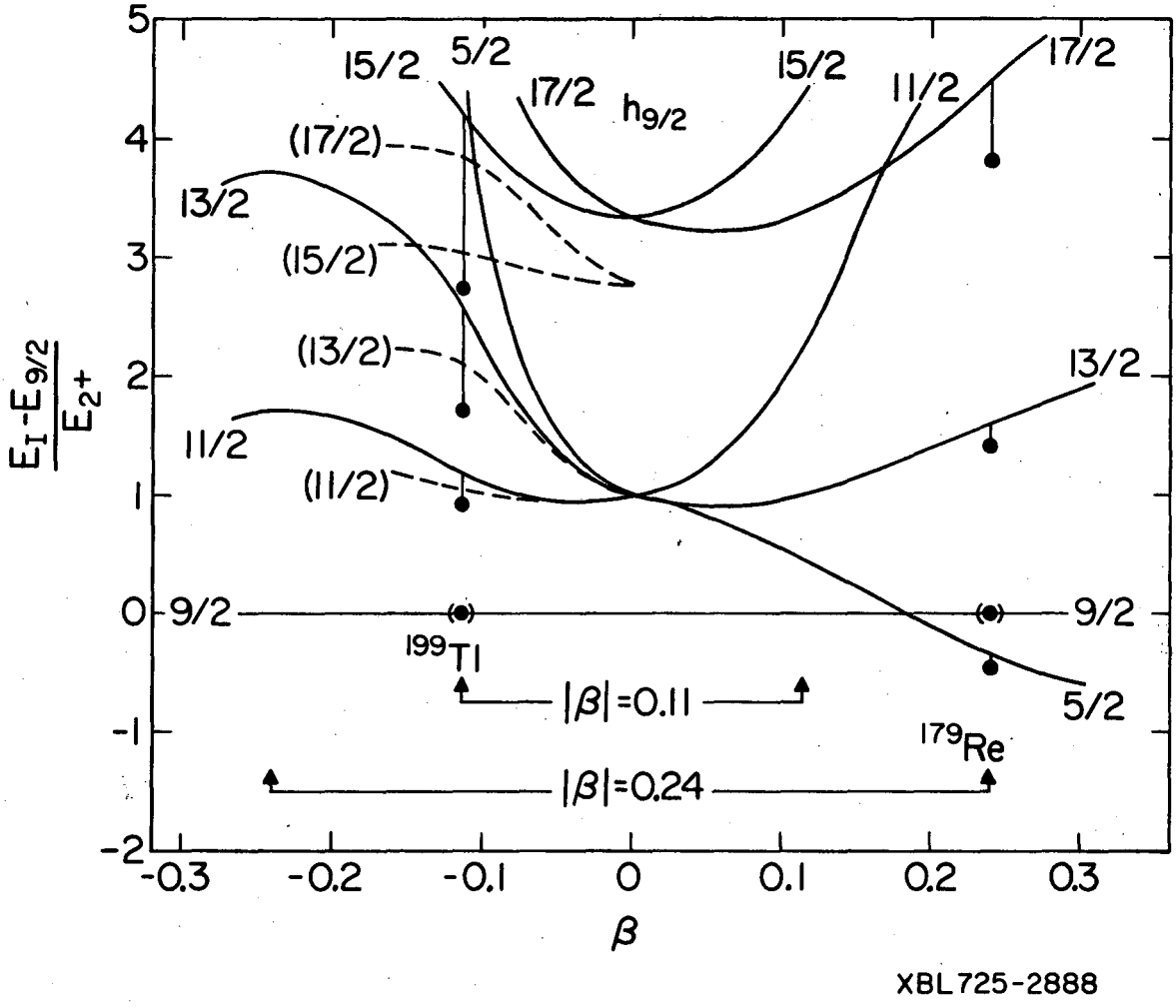
5
4
3
2
1
0
-1
-2
-0.3
-0.2
-0.1
0
0.1
0.2
0.3
β
$\frac{E_I - E_{9/2}}{E_{2^+}}$
15/2
5/2
17/2
$h_{9/2}$
15/2
11/2
17/2
(17/2)
13/2
(15/2)
(13/2)
13/2
11/2
(11/2)
9/2
9/2
^{199}Tl
|β|=0.11
5/2
^{179}Re
|β|=0.24
XBL725-2888

Fig. 16

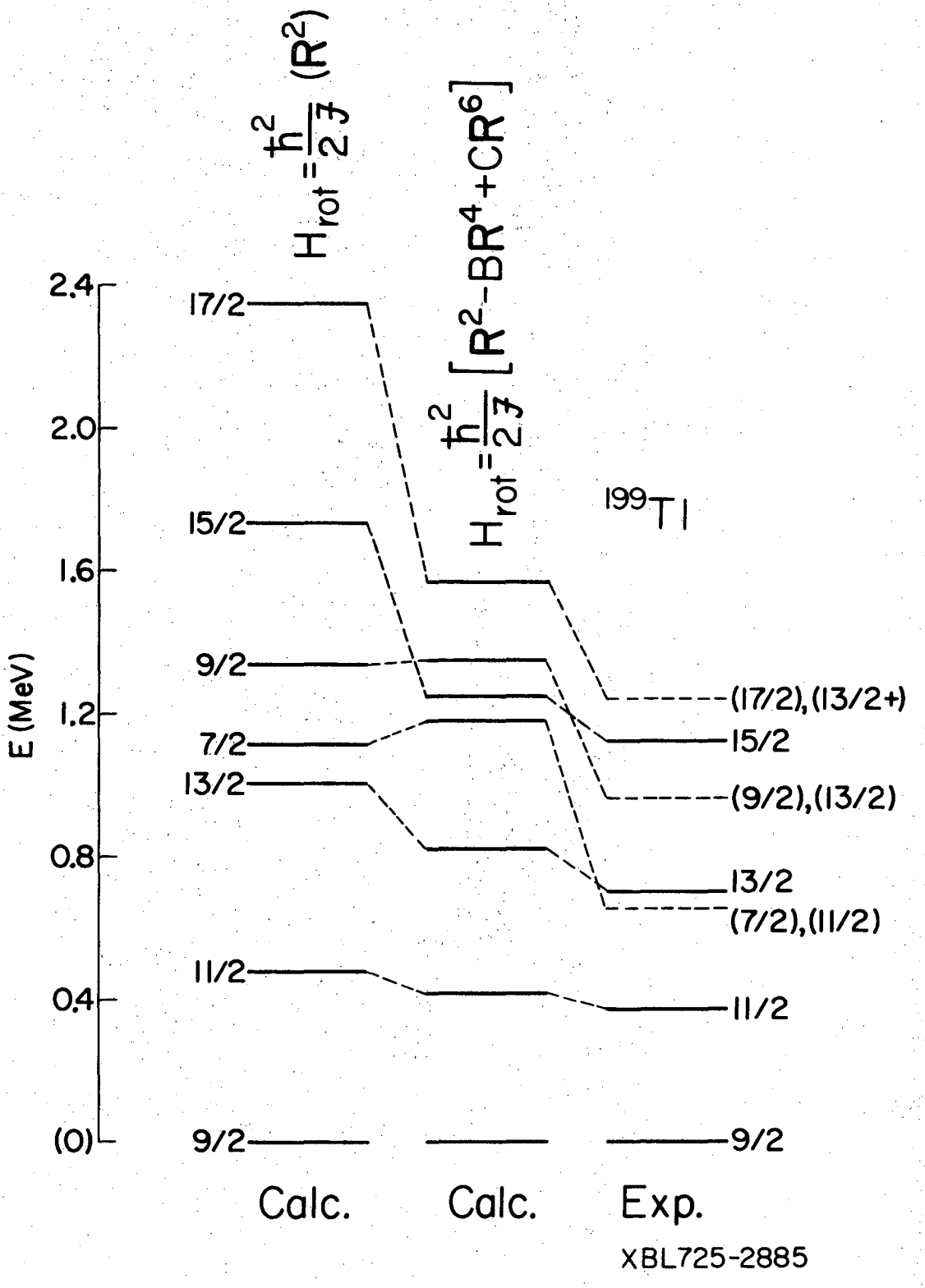
$H_{rot}=\frac{\hbar^2}{2\mathcal{J}}(R^2)$
$H_{rot}=\frac{\hbar^2}{2\mathcal{J}}[R^2-BR^4+CR^6]$
^{199}Tl
E (MeV)
2.4
2.0
1.6
1.2
0.8
0.4
(0)
17/2
15/2
9/2
7/2
13/2
11/2
9/2
(17/2),(13/2+)
15/2
(9/2),(13/2)
13/2
(7/2),(11/2)
11/2
9/2
Calc.
Calc.
Exp.
XBL725-2885

Fig. 17

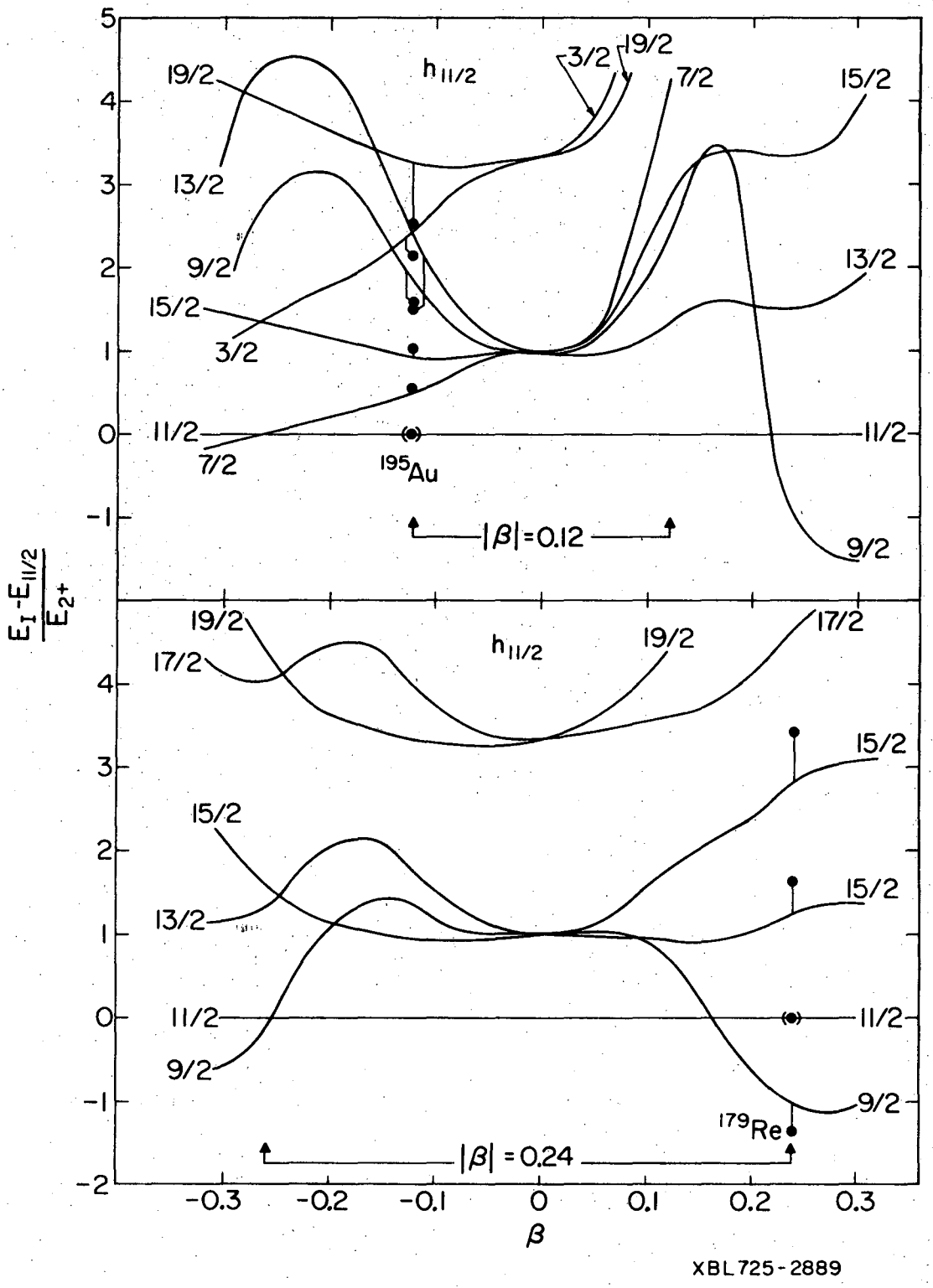
$\frac{E_I - E_{11/2}}{E_{2^+}}$
$h_{11/2}$
19/2
13/2
9/2
15/2
3/2
11/2
7/2
19/2
3/2
7/2
15/2
13/2
11/2
9/2
^{195}Au
$|\beta| = 0.12$
$h_{11/2}$
19/2
17/2
19/2
17/2
15/2
15/2
13/2
15/2
11/2
11/2
9/2
9/2
^{179}Re
$|\beta| = 0.24$
5
4
3
2
1
0
-1
-2
-0.3
-0.2
-0.1
0
0.1
0.2
0.3
β
XBL725-2889

Fig. 18

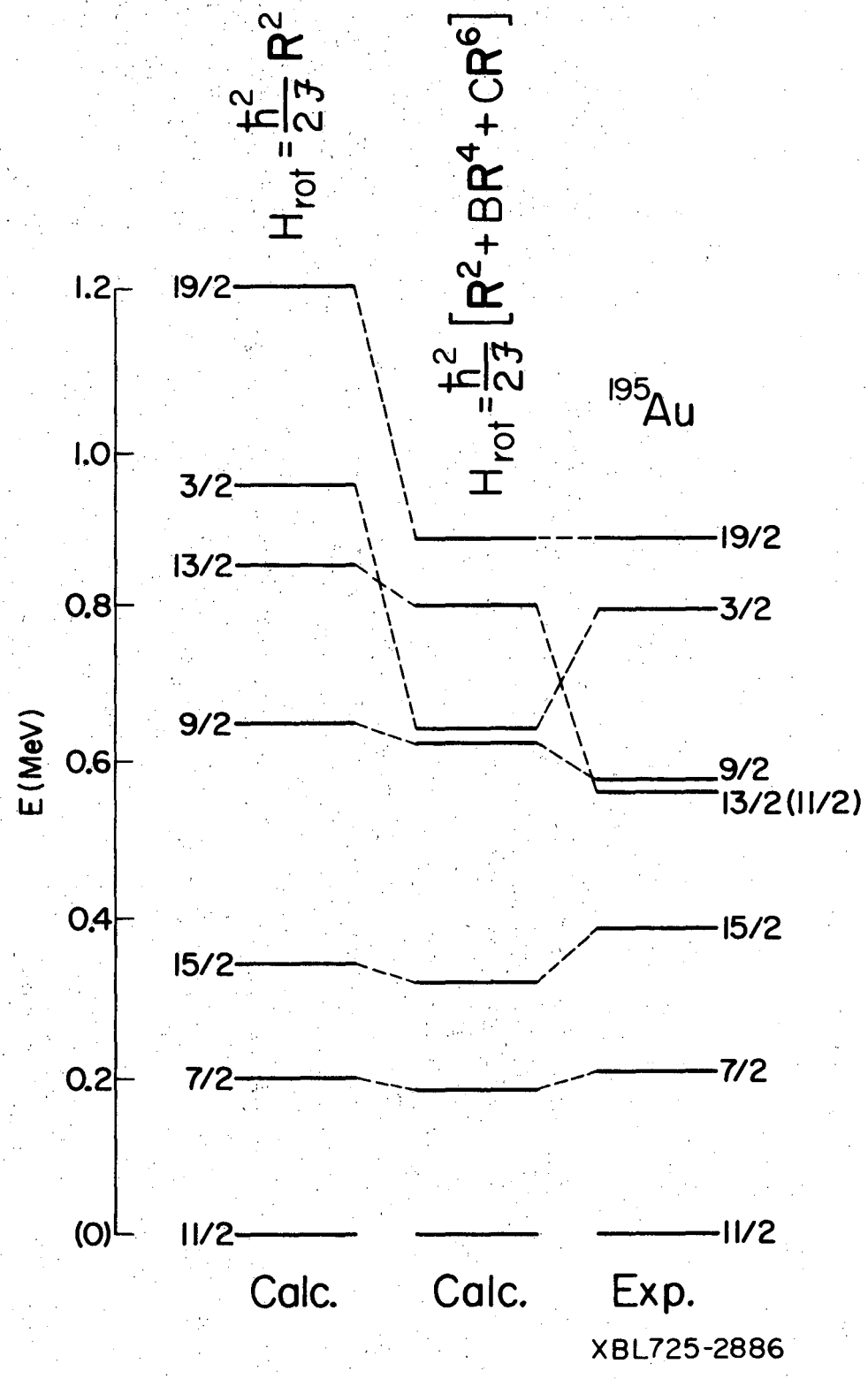
$H_{rot}=\frac{\hbar^2}{2\mathcal{J}}R^2$
$H_{rot}=\frac{\hbar^2}{2\mathcal{J}}[R^2+BR^4+CR^6]$
^{195}Au
E (MeV)
1.2
1.0
0.8
0.6
0.4
0.2
(0)
19/2
3/2
13/2
9/2
15/2
7/2
11/2
19/2
3/2
9/2
13/2 (11/2)
15/2
7/2
11/2
Calc.
Calc.
Exp.
XBL725-2886

Fig. 19

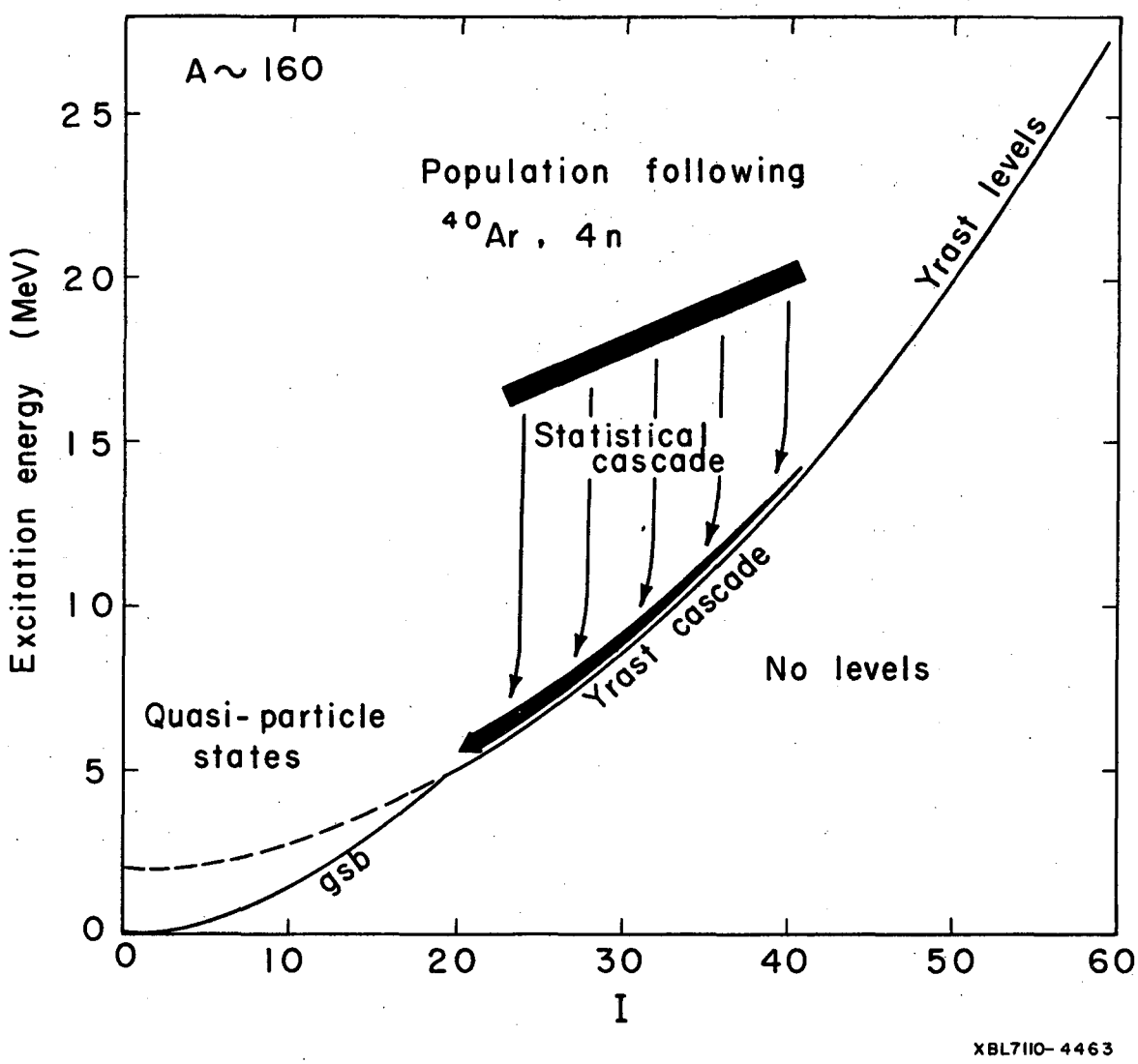
A ~ 160
Population following
40Ar , 4n
Yrast levels
Statistical cascade
Yrast cascade
No levels
Quasi-particle states
gsb
Excitation energy (MeV)
I
0
5
10
15
20
25
0
10
20
30
40
50
60
XBL7110-4463

Fig. 20

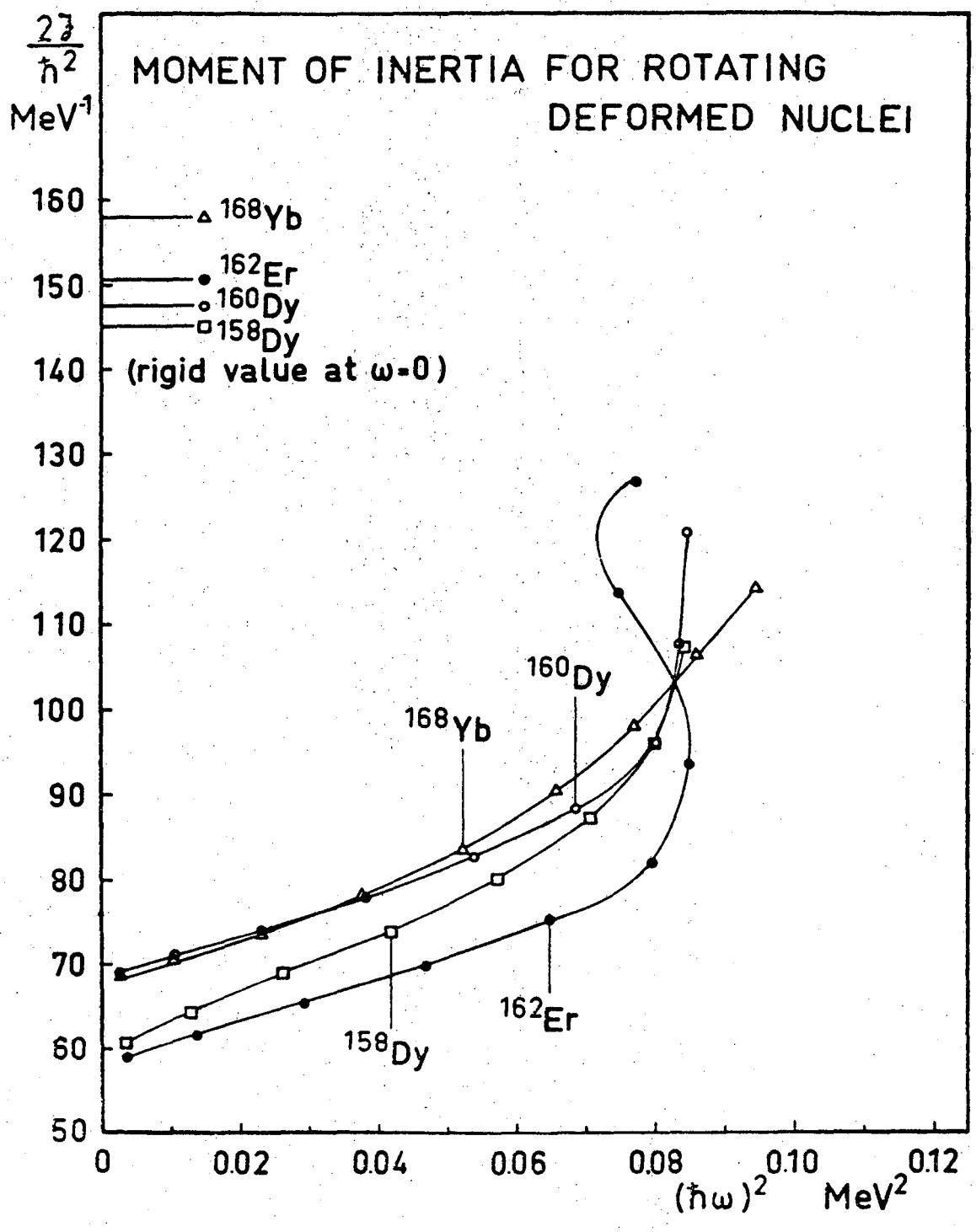
2ℑ/ħ²
MeV⁻¹
MOMENT OF INERTIA FOR ROTATING DEFORMED NUCLEI
168Yb
162Er
160Dy
158Dy
(rigid value at ω=0)
160
150
140
130
120
110
100
90
80
70
60
50
0
0.02
0.04
0.06
0.08
0.10
0.12
(ħω)² MeV²
XBL 728-1596

Fig. 21

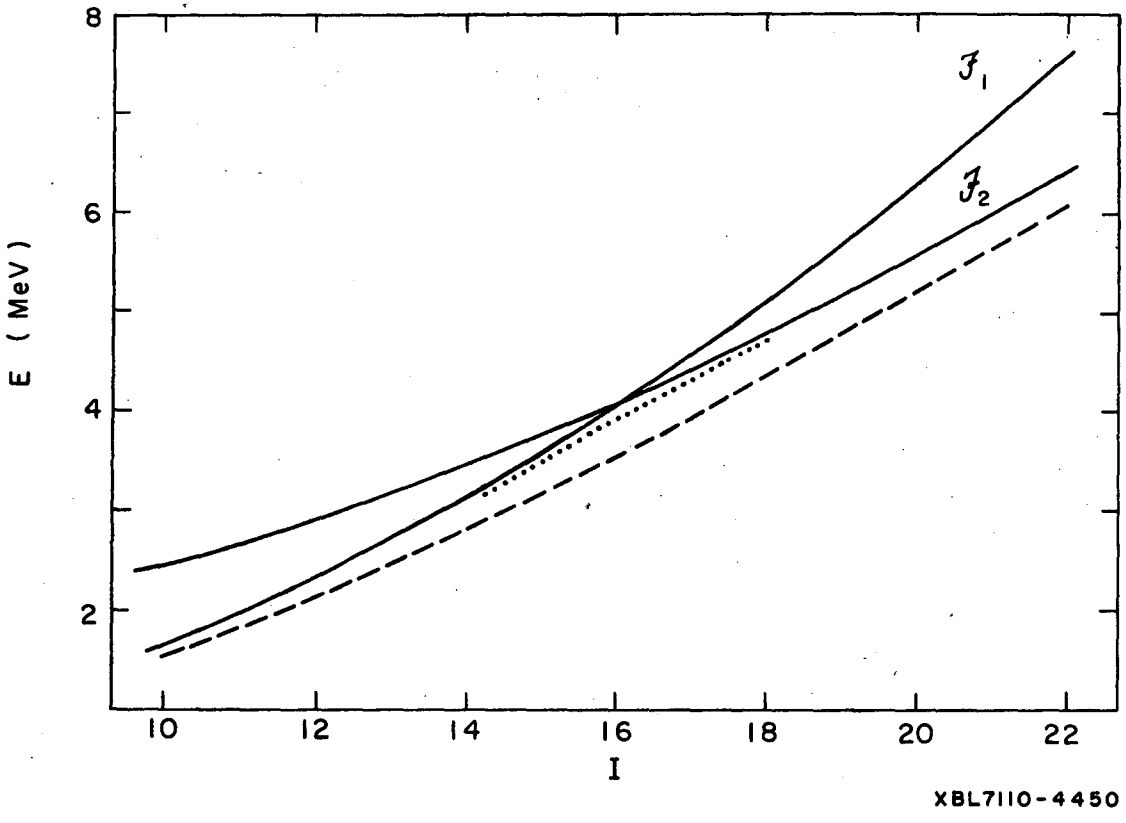
8
6
4
2
E (MeV)
10
12
14
16
18
20
22
I
$\mathcal{J}_1$
$\mathcal{J}_2$
XBL7110-4450

Fig. 22

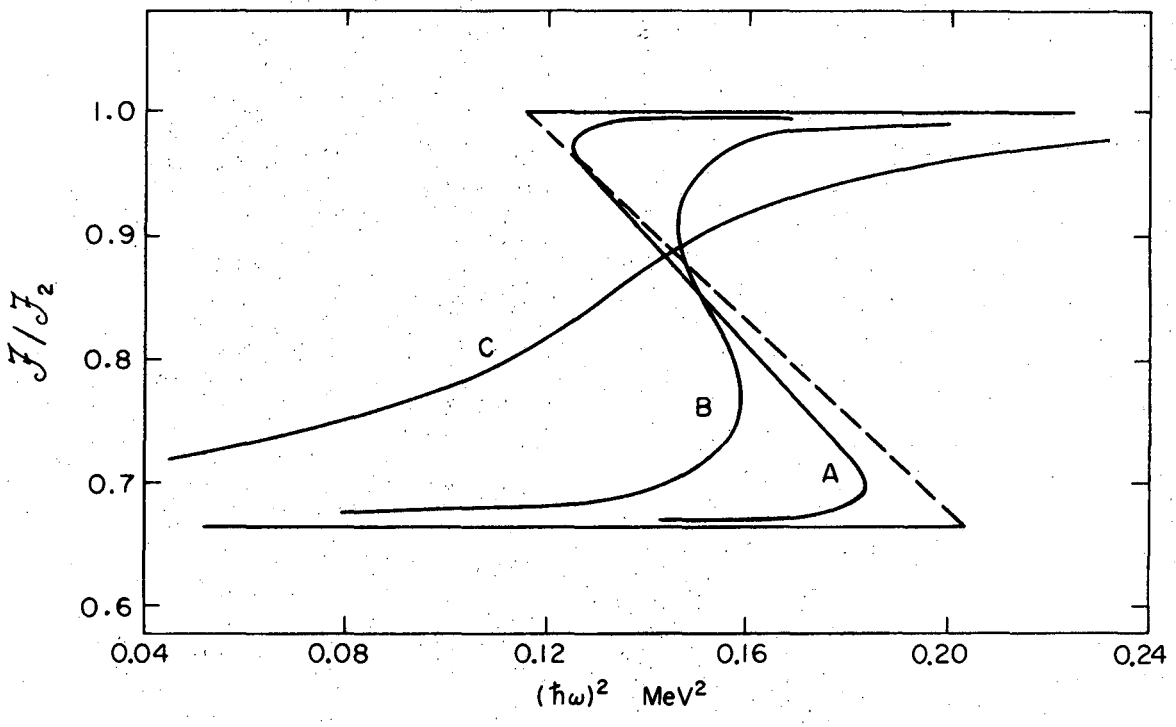
1.0
0.9
0.8
0.7
0.6
$\mathcal{J}/\mathcal{J}_2$
C
B
A
0.04
0.08
0.12
0.16
0.20
0.24
$(\hbar\omega)^2$ MeV^2
XBL7110-4451

Fig. 23

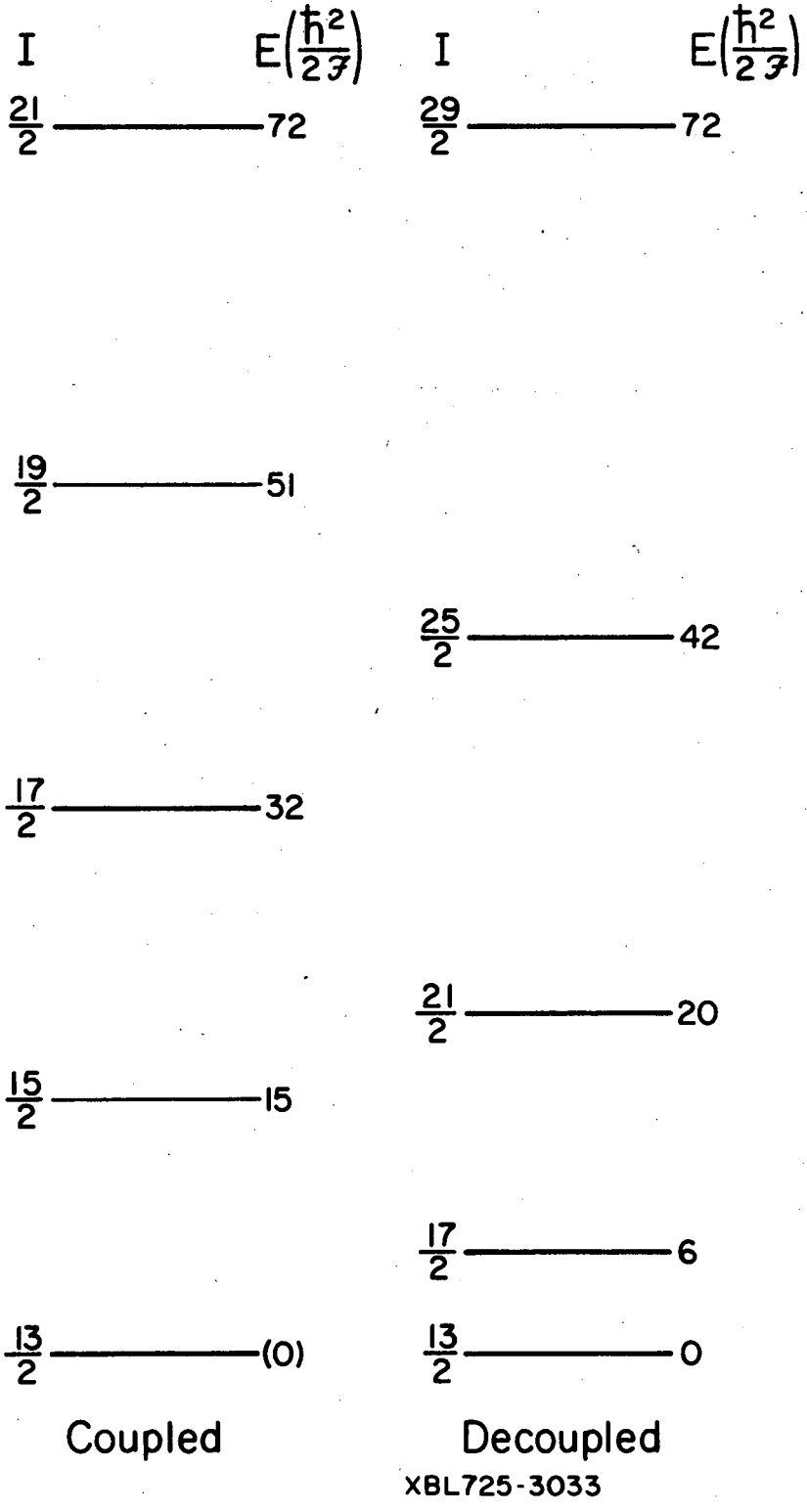
I
E(ħ²/2ℑ)
21/2
72
19/2
51
17/2
32
15/2
15
13/2
(0)
Coupled
I
E(ħ²/2ℑ)
29/2
72
25/2
42
21/2
20
17/2
6
13/2
0
Decoupled
XBL725-3033

Fig. 24

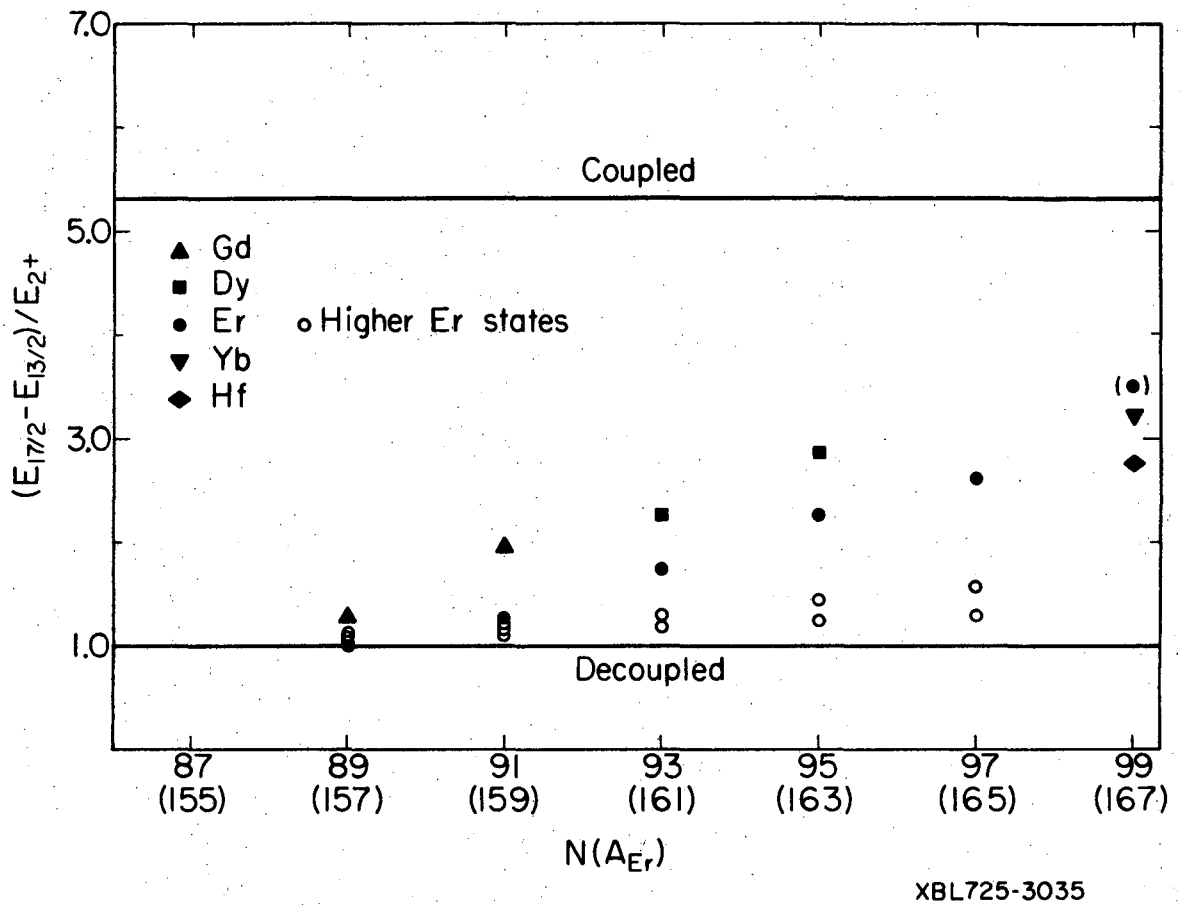
7.0
5.0
3.0
1.0
Coupled
Decoupled
▲ Gd
■ Dy
● Er
▼ Yb
◆ Hf
o Higher Er states
8
(●)
87 (155)
89 (157)
91 (159)
93 (161)
95 (163)
97 (165)
99 (167)
N(A_Er)
(E_17/2 - E_13/2)/E_2+
XBL725-3035

Fig. 25

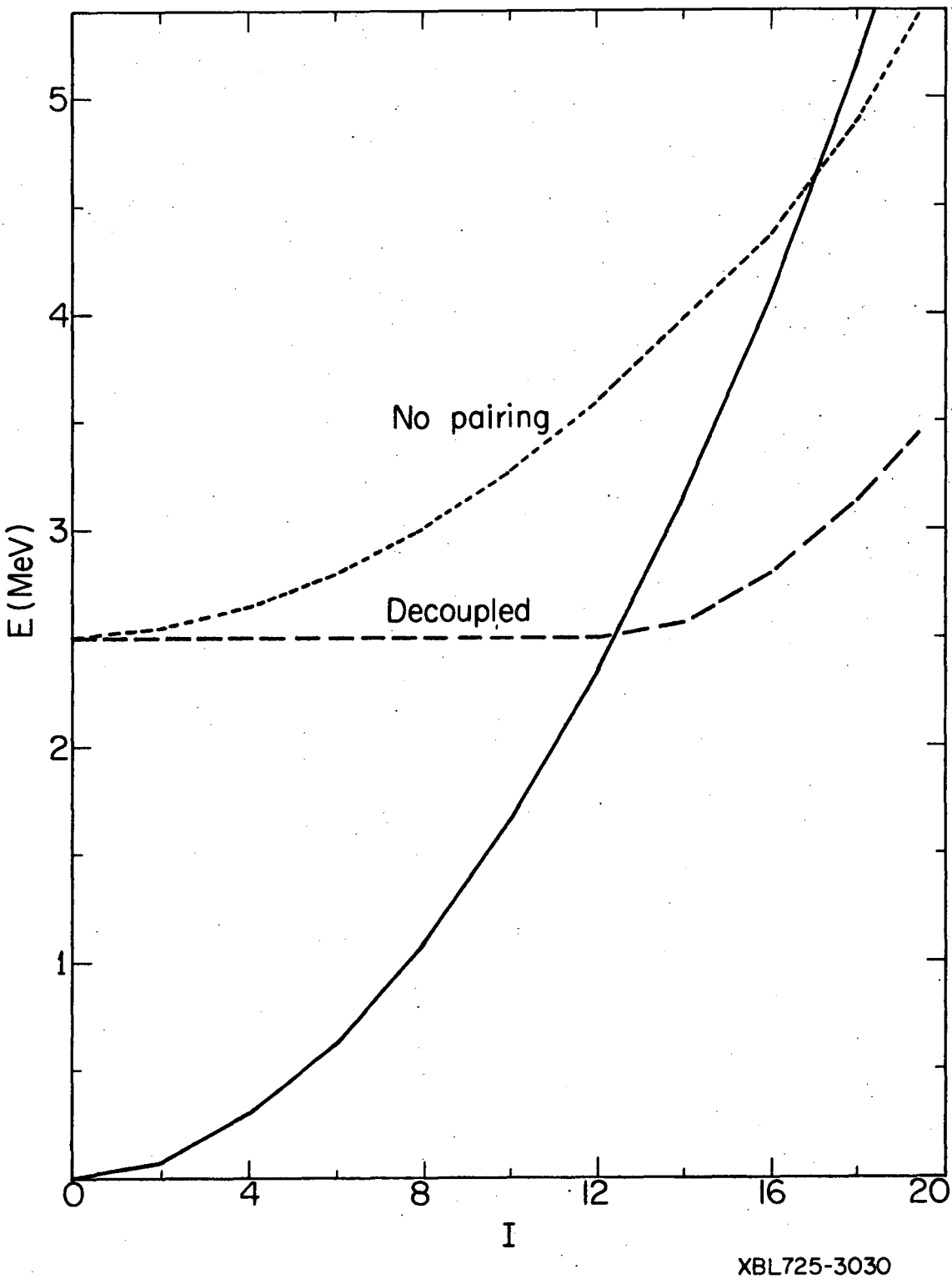

Fig. 26

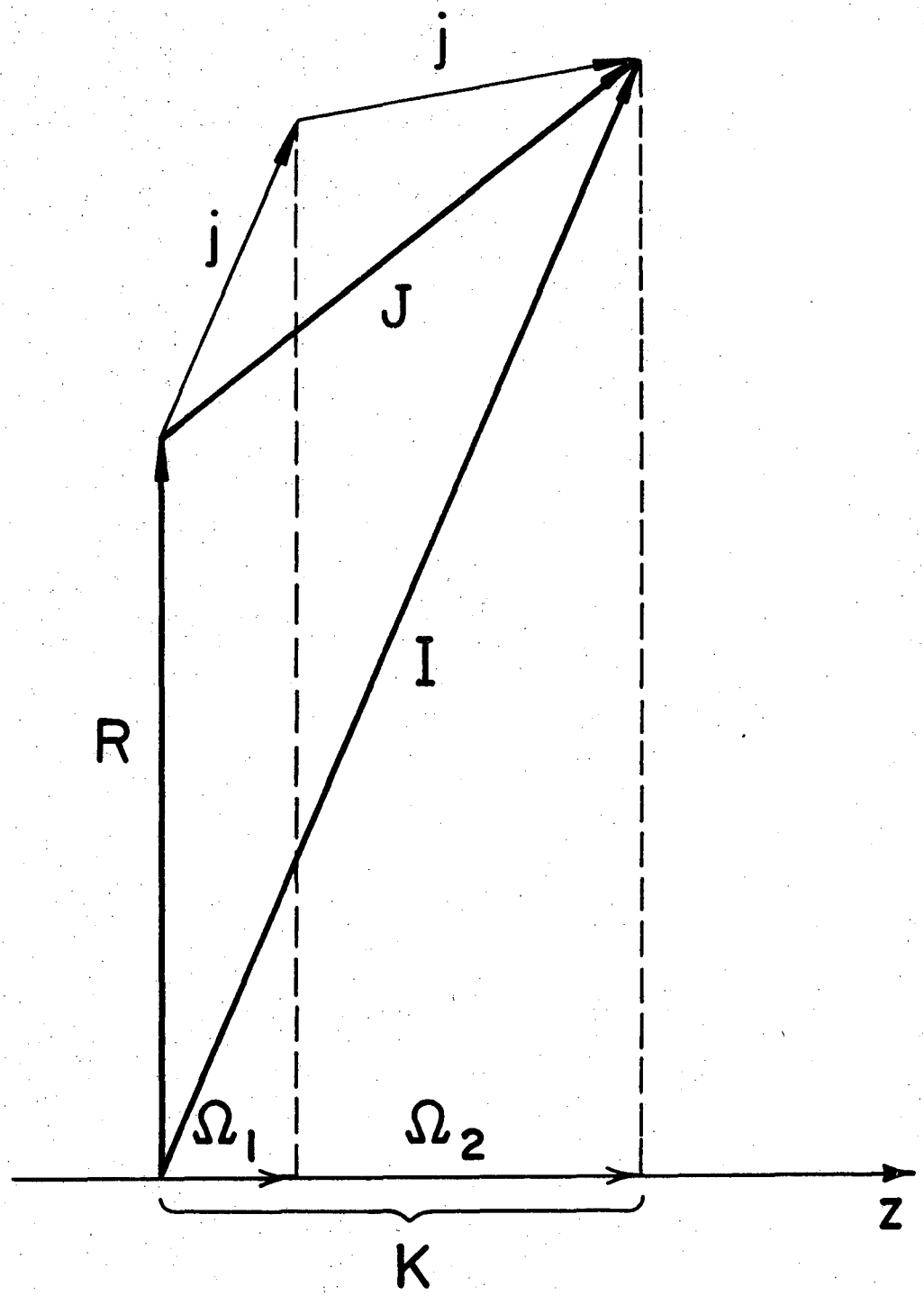

XBL 7110-4459

Fig. 27

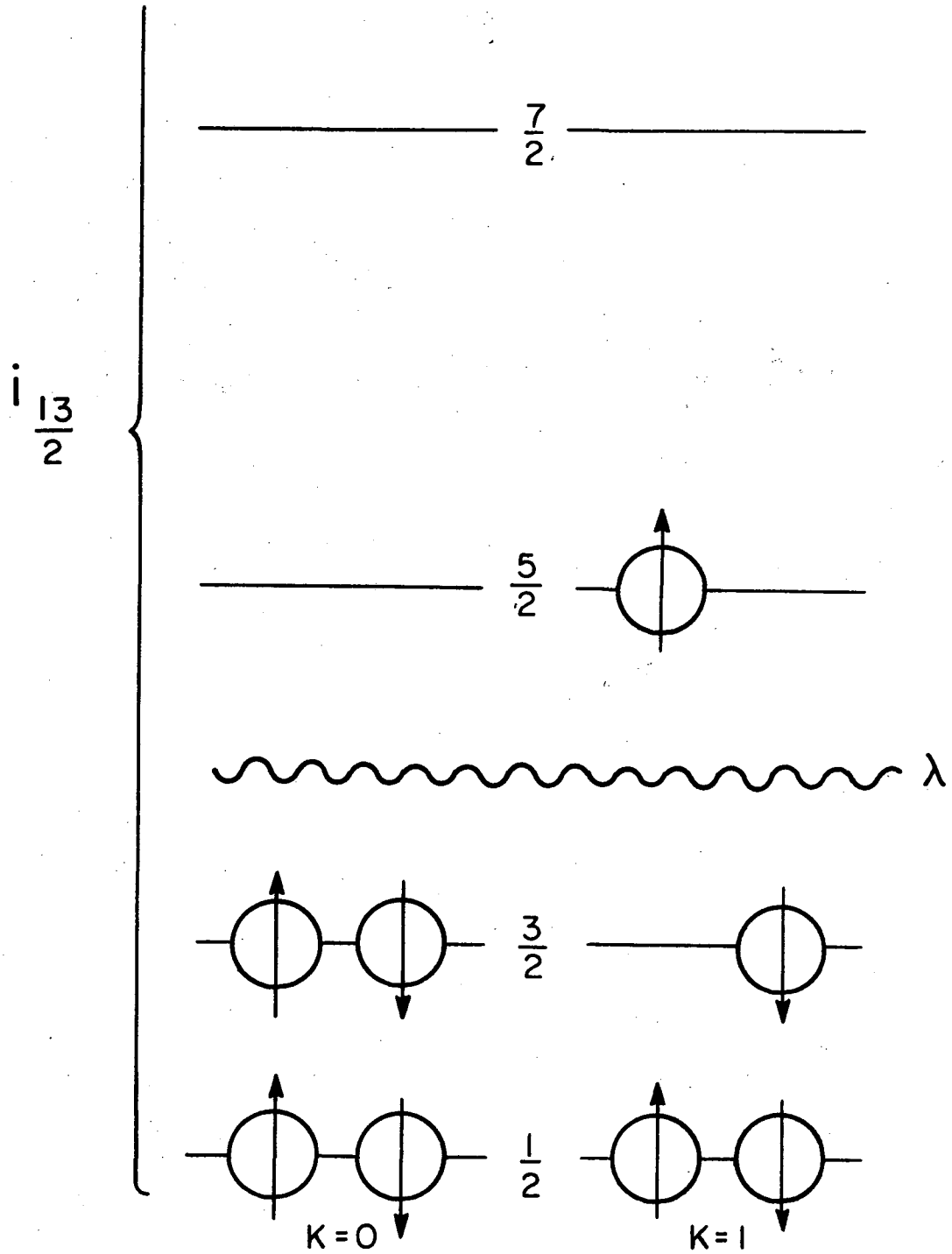

Fig. 28

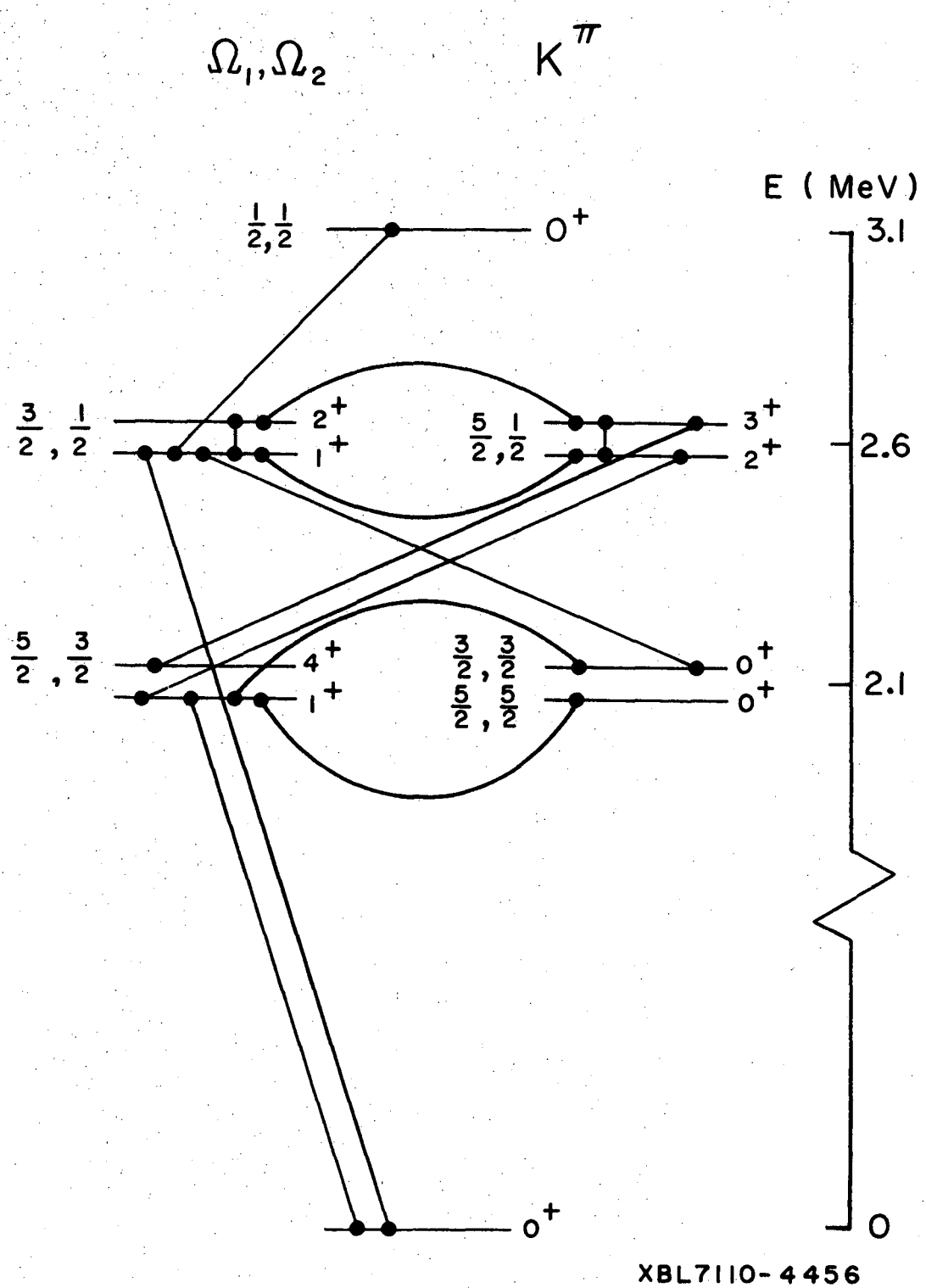
Ω_1, Ω_2
K^π
E (MeV)
3.1
2.6
2.1
0
$\frac{1}{2},\frac{1}{2}$ 0^+
$\frac{3}{2},\frac{1}{2}$ 2^+ 1^+
$\frac{5}{2},\frac{1}{2}$ 3^+ 2^+
$\frac{5}{2},\frac{3}{2}$ 4^+ 1^+
$\frac{3}{2},\frac{3}{2}$ 0^+
$\frac{5}{2},\frac{5}{2}$ 0^+
0^+
XBL7110-4456

Fig. 29

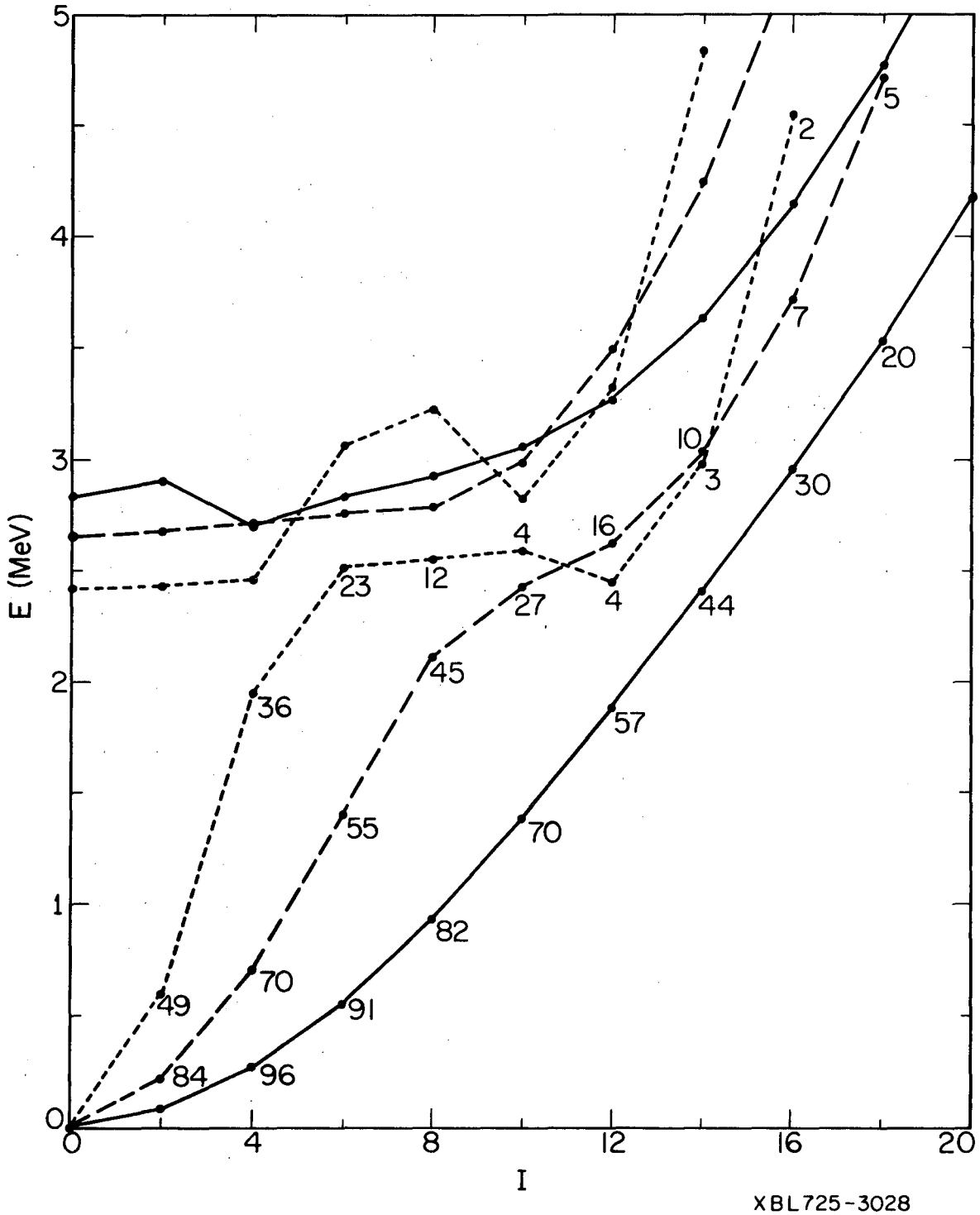
E (MeV)
I
0
1
2
3
4
5
0
4
8
12
16
20
49
84
36
70
23
55
12
45
4
27
16
4
10
3
2
5
7
20
30
44
57
70
82
91
96
XBL725-3028

Fig. 30

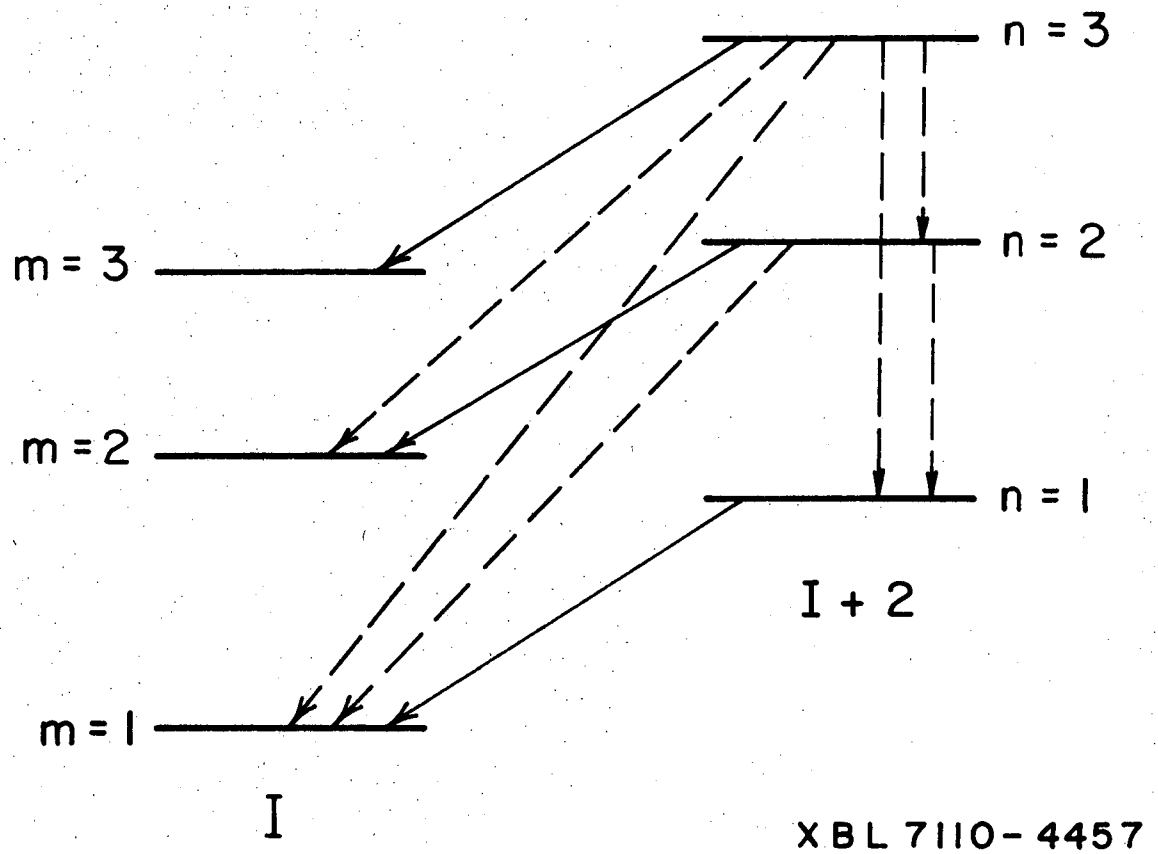

Fig. 31

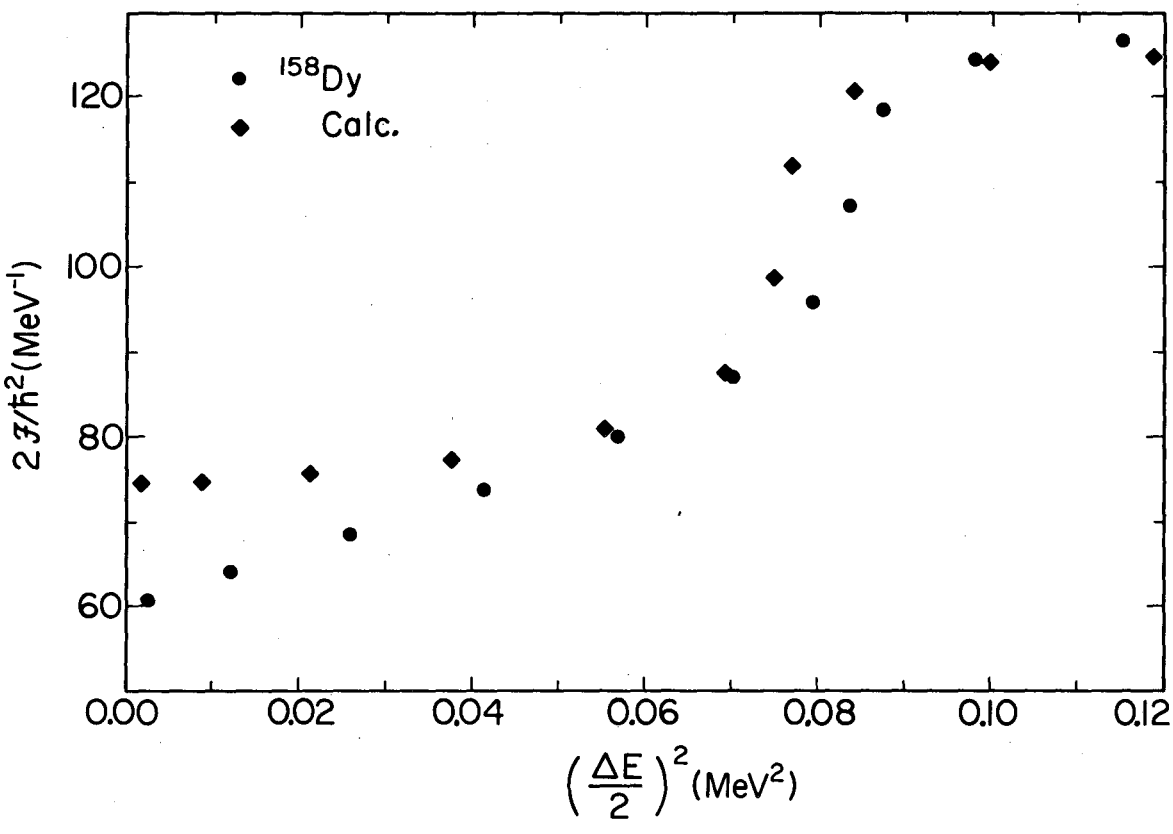
^{158}Dy
Calc.
120
100
80
60
$2\mathcal{I}/\hbar^2$(MeV^{-1})
0.00
0.02
0.04
0.06
0.08
0.10
0.12
$\left(\frac{\Delta E}{2}\right)^2$(MeV^2)
XBL725-3038

Fig. 32

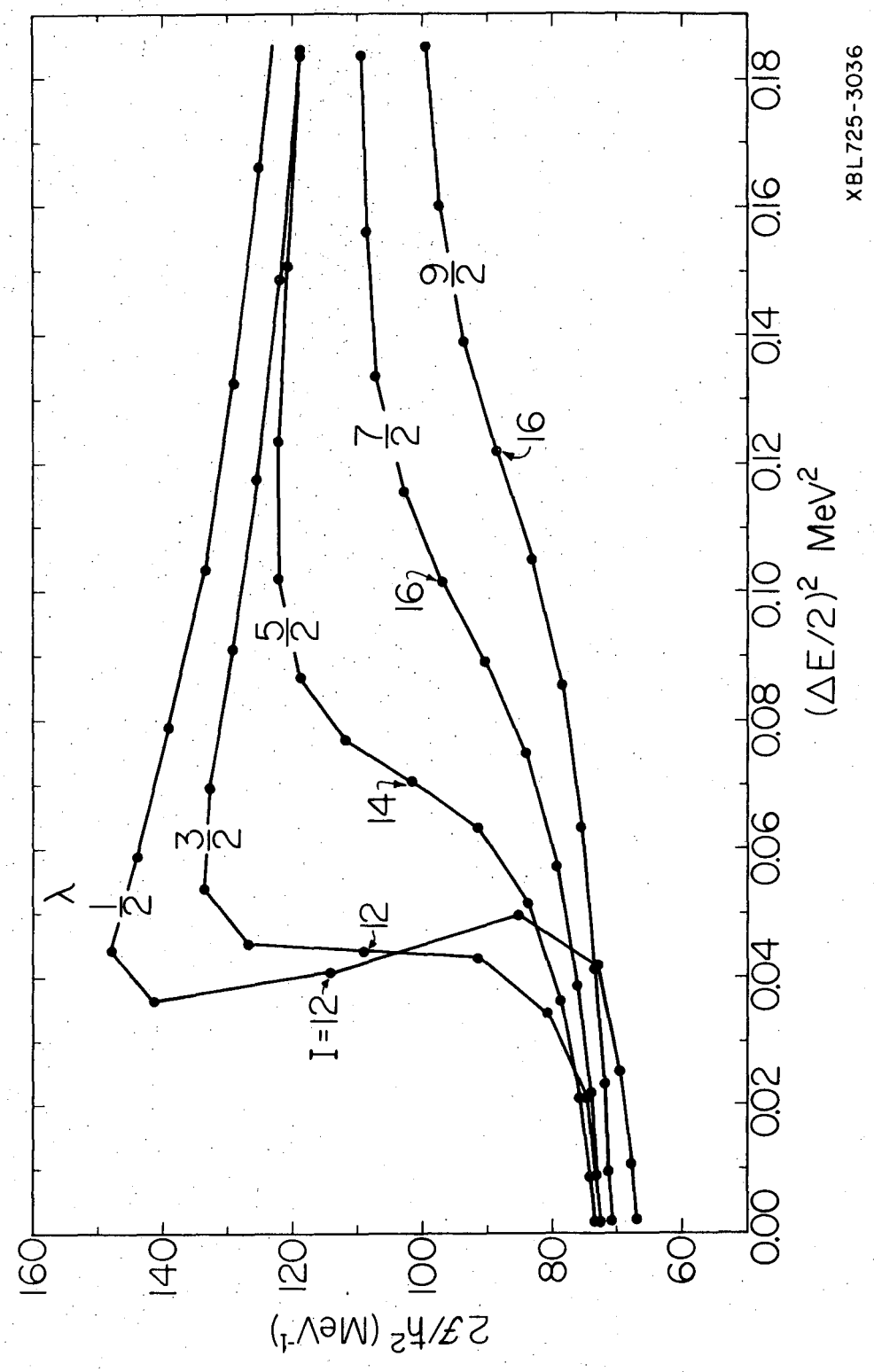
$2\mathcal{J}/\hbar^2$ (MeV^{-1})
160
140
120
100
80
60
0.00
0.02
0.04
0.06
0.08
0.10
0.12
0.14
0.16
0.18
$(\Delta E/2)^2$ MeV^2
γ
$\frac{1}{2}$
$\frac{3}{2}$
$\frac{5}{2}$
$\frac{7}{2}$
$\frac{9}{2}$
I=12
12
14
16
16
XBL725-3036

Fig. 33

TECHNICAL INFORMATION DIVISION
LAWRENCE BERKELEY LABORATORY
UNIVERSITY OF CALIFORNIA
BERKELEY, CALIFORNIA 94720